Master of Science

Enhancing the Chemically-Induced Optical Properties Supported by the Localized Surface Plasmon Resonance in Anisotropic Single Gold Bipyramids.

The Graduate School
of the University of Ulsan

Department of Chemistry
Philippe Tsalu Vuka

Enhancing the Chemically-Induced Optical Properties Supported by the Localized Surface Plasmon Resonance in Anisotropic Single Gold Bipyramids.

Advisor: Ji Won Ha

DISSERTATION

Submitted to
the Graduate School of Chemistry of the University of Ulsan
In partial fulfillment of the Requirements
for the Degree of

MASTER OF SCIENCE

By

Philippe Tsalu Vuka

Department of Chemistry
Ulsan, Korea
November 2018

Enhancing the Chemically-Induced Optical Properties Supported by the Localized Surface Plasmon Resonance in Anisotropic Single Gold Bipyramids.

This certifies that the dissertation/master thesis
is approved

Prof. Youngil Lee

Committee Chair Dr,

Prof. Ji Won Ha

Committee Advisor Dr,

Prof. Jong Wook Hong

Committee Member Dr

Department of Chemistry
Ulsan, Korea
November 2018

ACKNOWLEDGMENTS

I would deeply like to express my gratitude and appreciation to my advisor Prof. Ji Won Ha, from the University of Ulsan (UOU) for having welcomed me into the Advanced Nano-Bio-Imaging and Spectroscopy (ANBIS) laboratory, for my initiation to this field of *Nanoplasmonics* in chemistry and for his guidance that led to the realization of this dissertation. All i have lent from him are appreciated and will not be forgotten. May the almighty God grace rewards all his efforts.

My sincere acknowledgements and gratitude are also express to the National Institute for International Education (NIIED) and the Republic of Korea (South Korea) Ministry of Education, for the scholarship award funded by the Korean Government Scholarship Program (KGSP). Thank you for giving me the opportunity to learn new languages, new cultures and a new field. May the future of the Republic of Korea be more prosperous and its relationship with my country, the Democratic Republic of the Congo (DR Congo), be flourishing.

I want to thank all my senior labmates in ANBIS laboratory, for their support over the past two years. In particular, Geun Wan Kim and Seo Young Lee for the Dark Field microscopy and spectroscopy training.

I would also like to acknowledge and thank here Prof. Zephyrin Yav Gushimana, Prof. Pius Mpiana Tshimankinda and Prof. Tharcisse Monama Ondongo,from the University of Kinshasa (Unikin) in DR Congo, for having helped me to make precious first steps in researches and for having enabled me to stand onto your giants scientific shoulders to see far away. All i have lent from them are appreciated and may your advices, love and willingness be acknowledged by the almighty God grace.

To my wife Laurianne Akonda Zinga, for your commitment, patience, love, support and prayers during all the difficult and joyful times spent either separately or together, many thanks. And may the almighty God grace fructify our union. Many thanks also to our wedding witnesses Prof. Jeff Iteku Bekomo and Olga Nseya Mbombo for their tremendous support during the two first year of my

scholarship spent separately with my wife. Your support was deeply appreciated and will not be forgotten. Many thanks also to my friend Herve Pambu Phanzu, for your unforgettable attachment and support. And to Prof. Jules Tshishimbi Muya, thank you for your advices and support.

All my gratitude to Louis Kitenge Muyembe's family, especially to Marceline Kuta Kibangu for your endless love, support and everything you have done in my live. To Simon Kanda Mutabazi and Prof. Dorothee Tshilanda Dinangayi, thank you for your prayers, advices and support.

My high regard to professors Jong Wook Hong, Jaehoon Jung, SangKook Woo, Youngil Lee, Min Hyung Lee, Hyung-il Lee, Soon Cheol Hong, Achiri Celestine Tange at the University of Ulsan and Mudogo Virima, Kasende E. Okuma, Francois B. Kapuku, Mayaliwa Muzomwe, Gracien B. Ekoko, Omer M. Mvele at the University of Kinshasa, respectively.

I thanks also from the University of Kinshasa my friends Beaudrique M. Nsimba, Aristote P Matondo, Domaine T. Mwanangombo, and my seniors Didi D. Bibelayi, Pitchouna I. Kilunga and Albert S. Lundemba from the structural physical chemistry (SPS) laboratory for the good beautiful memories.

I finally thank my loved mother Bernadette Tshibuka Kumbi and all my family for the love and support.

Philippe Tsalu Vuka

To my family, I dedicate this work.

ABSTRACT

The localized surface plasmon resonance (LSPR)-based biosensors and others optical devices that employ gold nanoparticles (AuNPs) have shown tremendous advantages over techniques such as fluorescence and chemiluminescence in recent developments of nanoscience and nanotechnology. In one hand,the localized surface plasmon resonance (LSPR) biosensors are ultra-high refractive index sensing, they have a fast sensor response, they enable real-time detection and can be use in a label-free technique. In the other hand, instead surface plasmon resonance (SPR) in a bulk gold, gold nanoparticles (AuNPs) exploited under the quasi-static boundary condition offer an unprecedented platform for investigating on desired optical and spectroscopic properties at nanoscale. Relative to other metallic nanoparticles supporting LSPR signal, AuNPs have drawn the greatest attention and interest owing to their biocompatibility with high chemical and physical stability. More importantly, AuNPs easy functionalization with organic and biological molecules fostered their use as LSPR-based sensors materials. However, LSPR still has many fundamental limitations that cause LSPR based sensors efficiency to be low compared to surface plasmon polariton (SPP) sensors. One major limitation of LSPR sensor effectiveness is changes in the magnitude of the shift across the spectrum due to the shape of the LSPR peak when monitoring changes of the nanoparticle local environment at their surface. This results in unsymmetrical broadening and was found to have a negative impact on sensing efficiency. Therefore, for optimal and efficient engineering of gold nanoparticles (AuNPs) LSPR-based sensors and others optical devices, AuNPs LSPR based unique optical properties must be fully understood and harnessed.

As a first report, we devoted a particular focus on LSPR scattering inflection points (IFs) of single gold bipyramids (AuBPs). The findings reveal that tracking LSPR IFs exhibit high sensitivity over their counterpart LSPR peak shift locations. More importantly, the limitation on unsymmetrical broadening is no more a limitation on the changes of the magnitude of the shift across the spectrum due to the shape of the LSPR peak.

APPENDED PAPERS

The following work is included in this thesis:

Paper I

- Homogeneous Localized Surface Plasmon Resonance Inflection Points for Enhanced Sensitivity and Tracking Plasmon Damping in Single Gold Bipyramids, **Nanoscale, 2018,10, 12554–12563.(IF: 7.367)**

  Tsalu,P. V.; Kim, G. W.; Hong,J. W. and Ha, J. W.*

Other publications

The following work is related but not included in this thesis:

Paper II

- Single Particle Study: Size and Chemical Effects on Plasmon Damping at the Interface between Adsorbate and Anisotropic Gold Nanorods, **Phys. Chem. Chem. Phys., 2018,20, 22197-22202.(IF: 4.123)**

  Moon, S. W.; **Tsalu, P. V.**; Ha, J. W.

OUTLINE

CHAPTER 1:

GENERAL INTRODUCTION

1.1. Motivation and Background

Recent developments of nanoscience and nanotechnology have seen a tremendous growth in biosensors based on optical transducer principles. For instances, techniques such as fluorescence, surface plasmon resonance (SPR) and chemiluminescence were developed and widely used in enormous applications and optical devices [1]. In bio-sensing, SPR-based optical biosensors show numerous advantages over conventional sensors. SPR biosensors are ultra-high refractive index sensing, they have a fast sensor response, they enable real-time detection and can be use in a label-free technique [1, 2].

Instead of SPR in a bulk gold, gold nanoparticles (AuNPs) exploited under the quasi-static boundary condition offer an unprecedented platform for investigating on desired optical and spectroscopic properties at nanoscale [1-3]. Indeed, AuNPs smaller than their excitation wavelength, defined as quasi-static condition, LSPR. Under these subwavelength structure conditions, not only are electrons polarized and resonate, but the local electromagnetic field is enhanced [3, 4]. When illuminated by light with appropriate wavelength and polarization, the LSPR in AuNPs arises as a collective or coherent oscillation of conduction electrons. This generates local hot spots of high electric field accompanied by strong absorption, scattering, as well as several enhanced other optical properties [3, 5]. Relative to other metallic nanoparticles supporting LSPR signal, AuNPs have drawn the greatest attention and interest owing to their biocompatibility with high chemical and physical stability. More importantly, AuNPs easy functionalization with organic and biological molecules fostered their use as LSPR-based sensors materials [3].

Over many years, LSPR has been intensively investigated, which has permitted the optical properties of nanoparticles to be monitored by conventional UV-Visible spectroscopy and far-field techniques. Currently, LSPR has a variety of applications ranging from spectroscopy [3, 6], such as surface enhanced Raman

spectroscopy (SERS) [7]; to sensing [8], for instance plasmon-enhanced fluorescence [9], SERS and other techniques, and energy devices [10] as plasmonic solar cells [11], to photonics [12, 13], for example nanoscale lasers [14] and metamaterials [15]. Therefore, this broad range of advantages and applications has stimulated and fostered their use in bio and chemical LSPR based sensors.

Otherwise, LSPR excitation on an ensemble sample of anisotropic AuNPs exhibits two resonant modes, the less polarizable but high energy transverse mode and the highly polarizable with low energy longitudinal mode [1, 16]. In contrast, with a single AuNP, only the highly polarizable longitudinal mode has a high probability of occurring [17]. Indeed, for chemically synthesized ensemble nanoparticles, the inherent inhomogeneity or polydispersity (distribution of size and shape) provide spectral information with hidden (average) or heterogeneous properties of individual nanoparticles. Tremendous advances in experimental techniques and computational modeling, with their relative efficiencies have permitted and facilitated overcoming this limitation on measuring average properties [18]. Therefore, with the measuring of homogeneous properties, LSPR investigation through various scattering/absorption/extinction-based single nanoparticle spectroscopy techniques is growing exponentially and gaining more attention, especially for anisotropic single nanoparticles with high polarizability such as gold nanorods (AuNRs) and bipyramids (AuBPs).

Moreover, the ability to monitor LSPR spectral characteristics at the ensemble and single nanoparticle levels has revealed that they are strongly dependent on the geometry, composition, and size of the nanoparticles as well as on their local environment. Control of these parameters has opened an unprecedented possibility of tuning plasmonic properties and engineering of light Generally, changes in resonance peaks result in a red shift as well as a broadening of peaks when the size of the nanoparticles or the local RI increases [1, 18]. The local nature RI sensitivity of LSPR has led to the development of nanoparticles as chemo- and biosensors. Fundamentally, LSPR sensors consist of functionalized particles with target molecule receptors, which LSPR shifts, dampens, or enhances in the presence of target molecules. These changes in nanoparticle optical properties signal the

presence of target molecules and facilitate monitoring LSPR by relying on the shift of the peak maximum, the intensity, and broadening of the peaks. Broadening arises from LSPR decay, also known as the damping or dephasing time through energy conversion or energy transfer [1, 3]. Although researchers have taken advantage of all of these tremendous applications, LSPR still has many fundamental limitations that cause LSPR based sensor efficiency to be low compared to surface plasmon polariton (SPP) sensors [3]. In AuNPs, the LSPR related optical properties accuracy determination are impacted by a realistic representation of the frequency dependent dielectric function of the nanoparticles. Therefore, simplistic models negatively impact the fundamental quantities that are necessary for the design and fabrication of reliable devices based on plasmonic resonances. A realistic representation of the frequency dependent dielectric function consists of intra-band and inter-band electronic (IB) transitions [3, 19]. The former account for free carriers, whereas the latter account for bound electrons. Because for metals, free carriers dominate, Drude-type models were reliably used to describe material properties for silver. However, applying this model to AuNPs does not work perfectly above a threshold where IB transitions should be corrected. In the visible and near infrared, 2.4 eV is the most used threshold to ignore the effect of IB transitions on gold plasmons [20]. Whereas in the same frequency range, Derkachova et al. reported 1.8 eV to be the threshold according to their experimental findings [19]. In attempting to correct IB transition contributions by use of the Lorentz bound electron model, Alabastri et al. showed that the threshold can vary depending on the resonance location [21]. In the literature, there are no studies that quantitatively provide IB transition contributions to the frequency range dominated by intra-band electronic transitions due to free carriers.

One other major limitation of LSPR sensor effectiveness is changes in the magnitude of the shift across the spectrum due to the shape of the LSPR peak when monitoring changes of the nanoparticle local environment at their surface. This results in unsymmetrical broadening and was found to have a negative impact on sensing efficiency [22]. Methods such as lithography have been attempted to improve efficiency, but they tended to be high cost, low yielding, and tedious to process.

In this work, I firstly for the first time introduced the LSPR inflection points (LSPR-IFs) in single AuNPs as a novel approach for overcoming the limitation due to LSPR shift minute changes and the lack of constancy in the magnitude of shifts in LSPR-based bio- chemical sensors, to improve the performance of the latter.

1.2. Thesis Outline

Out of the present chapter on the general introduction, the following parts of the present dissertation consist of chapter 3 which provide the general theoretical background on Nanoplasmonics and single particles study. Chapters 3 presents one scientific manuscripts including introduction, experimental section, results and discussion, cited literature, figures and supplementary information. Chapter 3 reports the Homogeneous Localized Surface Plasmon Resonance Inflection Points for Enhanced Sensitivity and Tracking Plasmon Damping in Single Gold Bipyramids. The thesis fence by a general conclusion.

1.3. References

1. Cao, J.; Sun, T.; Grattan, K.T.V.,Gold nanorod-based localized surface plasmon resonance biosensors: A review, Sensors and Actuators B: Chemical, 2014, 195, 332-351.
2. Amendola, V.; Pilot, R.; Frasconi, M.; Marago O. M. and Iati, M. A., Surface plasmon resonance in gold nanoparticles: a review, Journal of physics. Condensed matter : an Institute of Physics journal, 2017, 29, 203002.
3. Tsalu, P.V.; Kim, G.W.; Hong, J.W.; Ha J.W., Homogeneous localized surface plasmon resonance inflection points for enhanced sensitivity and tracking plasmon damping in single gold bipyramids, Nanoscale. 2018, 10, 12554-12563.
4. Jana, J.; Ganguly, M.; and Pal, T., Enlightening surface plasmon resonance effect of metal nanoparticles for practical spectroscopic application, RSC Advances, 2016, 6, 86174-86211.
5. Garcia-Rico, E.; Alvarez-Puebla, R.A.; and Guerrini, L., Direct surface-enhanced Raman scattering (SERS) spectroscopy of nucleic acids: from fundamental studies to real-life applications, Chem. Soc. Rev., 2018,47, 4909-4923.

6. Jeppesen, C.; Lindstedt, D.N.; Laurberg, A.V.; Kristensen A. and Mortensen, N.A.; Nanometrology using localized surface plasmon resonance spectroscopy, Proceedings of CLEO Europe 2013. IEEE, 2013. p. 1.2013.
7. Gabudean, A. M.; Biro D. and Astilean, S., Localized surface plasmon resonance (LSPR) and surface-enhanced Raman scattering (SERS) studies of 4-aminothiophenol adsorption on gold nanorods, Journal of Molecular Structure, 2011, 993, 420-424.
8. M. Chamanzar and A. Adibi, Compact fluorescence sensor using on-chip silicon nitride microdisk, IEEE Photonic Society 24th Annual Meeting, 2011.
9. M. Bauch, K. Toma, M. Toma, Q. Zhang and J. Dostalek, Plasmon-Enhanced Fluorescence Biosensors: a Review, Plasmonics, 2014, 9, 781-799.
10. Yonzon, C. R., Zhang, X., Van Duyne, R. P. (2003). Localized surface plasmon resonance immunoassay and verification using surface-enhanced Raman spectroscopy. Proceedings of SPIE - The International Society for Optical Engineering, 5224, 78-85.
11. Unser, S.; Bruzas, I.; He, J.; Sagle, L. Localized Surface Plasmon Resonance Biosensing: Current Challenges and Approaches. Sensors 2015, 15, 15684-15716.
12. Yokota, H.; Taniguchi, T.; Watanabe T. and Kim, D., Control of localized surface plasmon resonance energy in monolayer structures of gold and silver nanoparticles, Physical Chemistry Chemical Physics, 2015, 17, 27077-27081.
13. Gu, X.; Qiu, T.; Zhang W. and Chu, P.K. Light-emitting diodes enhanced by localized surface plasmon resonance, Nanoscale Research Letters, 2011, 6, 199-199.
14. Li, J.; Cushing, S.K.; Zheng, P.; Meng, F.; Chu D.; and Wu, N., Plasmon-induced photonic and energy-transfer enhancement of solar water splitting by a hematite nanorod array, Nature Communications, 2013, 4, 2651.
15. Yu, M.; Yang, C.; Li, X.-M.; Lei, T.-Y.; Sun, H.-X.; Dai, L.-P.; Gu, Y.; Ning, X.; Zhou, T.; Wang, C.; Zeng H.-B.; and Xiong, J., Universal liquid-phase laser fabrication of various nano-metals encapsulated by ultrathin carbon shells for deep-UV plasmonics, Nanoscale, 2017, 9, 8716-8722
16. Bok, H. M.; Shuford, K. L.; Kim, S.; Kim S. K. and Park, S., Multiple Surface Plasmon Modes for Gold/Silver Alloy Nanorods, Langmuir: the ACS journal of surfaces and colloids, 2009, 25, 5266-5270.

17. Schneider, T.; Jahr, N.; Jatschka, J.; Csaki, A.; Stranik O. and Fritzsche, W., Localized surface plasmon resonance (LSPR) study of DNA hybridization at single nanoparticle transducers, Journal of Nanoparticle Research, 2013, 15, 1531.
18. Olson, J.; Dominguez-Medina, S.; Hoggard, A.; Wang, L.-Y.; Chang W.-S. and Link, S., Chemical Society reviews, 2015, 44, 40-57.
19. Derkachova, A; Kolwas, K; Demchenko, I., Dielectric Function for Gold in Plasmonics Applications: Size Dependence of Plasmon Resonance Frequencies and Damping Rates for Nanospheres, Plasmonics. 2016, 11, 941-951.
20. Foerster, B; Joplin, A; Kaefer, K; Celiksoy, S; Link, S; Sönnichsen, C., Chemical Interface Damping Depends on Electrons Reaching the Surface, ACS Nano, 2017, 11, 2886-2893.
21. Alabastri, A.; Tuccio, S.; Giugni, A.; Toma, A.; Liberale, C.; Das, G.; Angelis, F.; Fabrizio, E. D. and Zaccaria, R. P., Molding of Plasmonic Resonances in Metallic Nanostructures: Dependence of the Non-Linear Electric Permittivity on System Size and Temperature, Materials (Basel, Switzerland), 2013, 6, 4879-4910.
22. Chen, P.; Tran, N. T.; Wen, X.; Xiong Q. and Liedberg, B., ACS sensors, 2017, 2, 235-242.

CHAPTER 2:

THEORETICAL BACKGROUND

1. Historic Glimpse on gold nanoparticles.

Noble metal nanoparticles, especially Gold nanoparticles (AuNPs) with their varieties of optical and spectroscopic properties have been formerly used since ancient times to make stained glass (See Figure 1A-1C) and other products made by humans [1, 2]. However, for AuNPs it was long assumed that the different colors of the various gold suspensions were a result of the chemicals utilized to prepare those suspensions. From 1857 with the development of electromagnetic theory and experimental approaches, Michael Faraday produced the first pure samples of gold colloids and discovered that their colors were due to the size (Figure 1D) of the gold particles [2].

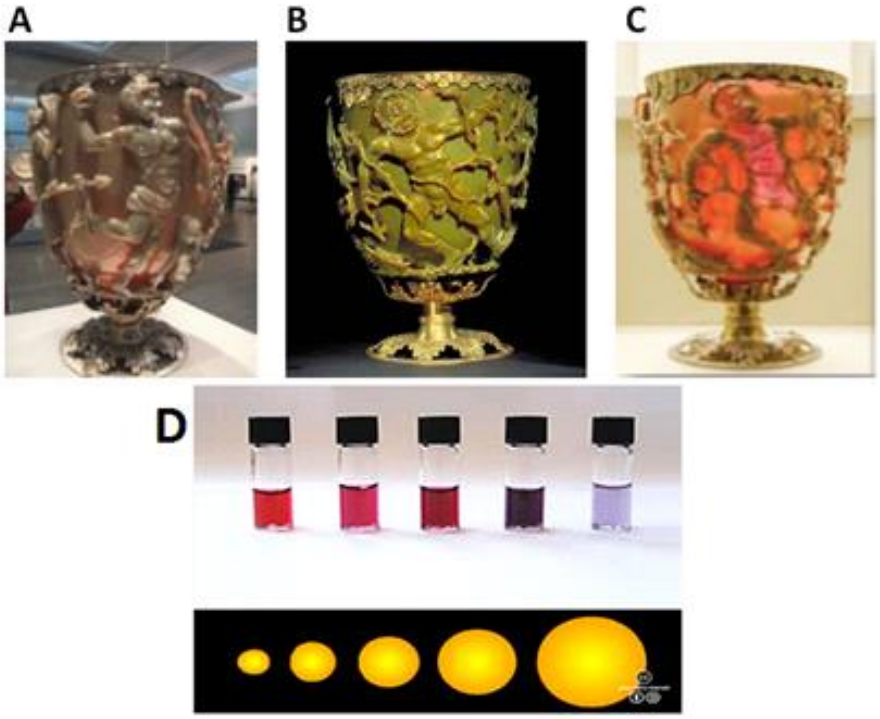

Figure 1. *The 4th-century Roman Lycurgus Cup at the British Museum absorbs and scatters blue and green light so that it shows a red color when the white light is*

placed inside the cup (A) or in reflected light mode, but appears green hue when the white light is incident from the outside (B) or in transmitted light mode and a mix of reflected and transmitted light. Reprinted from the reference 1 and 2. (D) Gold nanosphere color as function of size.

Nowadays not only nanoparticles in general, but also especially those of gold are extensively studied for the distinct properties that they can exhibit at the nanoscale. However, in reality, such brilliant colors of stained glass, luster of jewelry, and reflection of images in mirrors all owe their unique visual properties to the free electron gas character of the noble metals, whose behaviors changes with respect to their sizes when interacting with the electromagnetic field of visible light. In fact, the ease of mobility of these carriers (free electrons) enable these materials to readily respond to visible light, even when such materials are shrunk down to nanoscopic dimension into individual nanoparticles and their assemblies [3]. Such a response to light at the nanoscale exhibit a signal known as surface '*plasmon*'. To date plasmon is implicated in various application areas ranging from surface-enhanced molecular spectroscopy and sensing to photothermal cancer therapy and plasmon-driven photochemistry [1, 3].Plasmon has become an entire field called '*Plasmonics*' and is exponentially growing [4]. In the following section we introduce the fundamental basic of *plasmon*. Our focus is mainly orientated on gold nanoparticles (AuNPs) as noble metals.

2. Surface plasmon and localized surface plasmon

Plasmon is a quantum of plasma oscillation which is sometimes called the fourth state of matter. Plasma is created by adding energy to a gas so that some of its electrons leave its atoms [1, 5]. Plasmons are oscillations in the plasma of free electrons that constantly swirl across the surface of conductive materials like metals. In some nanomaterials, a specific color of light can resonate with the plasma and cause the electrons inside it to lose their individual identities and move as one, in rhythmic waves (Figure 2A-2B) [5]. Two kinds of plasmons can be distinguish depending on the materials size. In one hand surface plasmon polaritons (SPP), when the electromagnetic (EM) excitation propagates at the interface between a dielectric and a metal (Figure 2A), or in a metal surface-confined EM radiation interact with

molecular surface layer [1]. In the other hand, localized surface plasmon resonance (LSPR), when the metallic particles are smaller than the incident wavelength of radiation, giving rise to plasmon that oscillate locally around the nanoparticle (Figure 2B). Indeed, AuNPs smaller than their excitation wavelength, defined as quasi-static approximation, exhibit LSPR [6, 8]. When illuminated by light with appropriate wavelength and polarization, the LSPR in AuNPs arises as a collective or coherent oscillation of conduction electrons (Figure 2B).

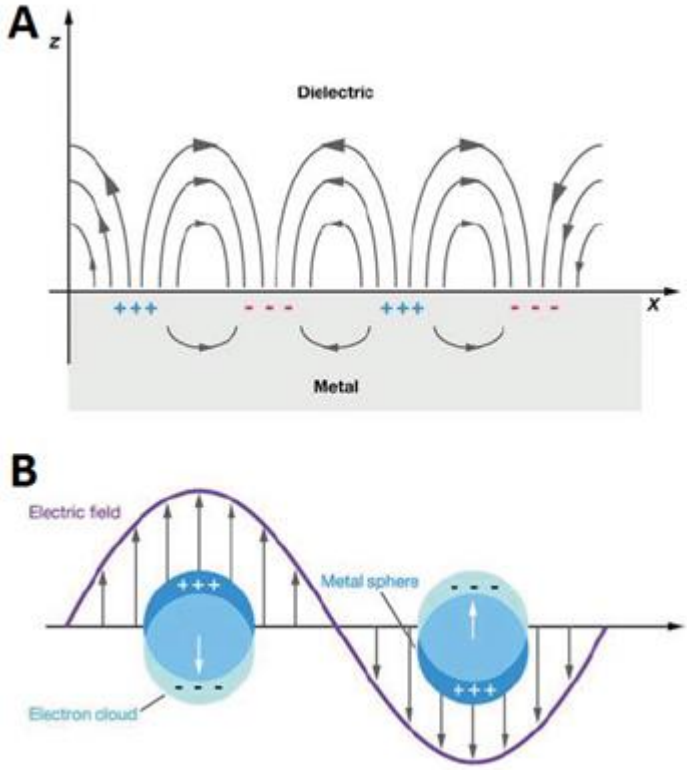

Figure 2. *The light resonates with the plasma and cause the electrons inside it to lose their individual identities and move as one, in rhythmic waves or collective or coherent oscillation of conduction electrons. Reprinted from reference 6.*

This generates local hot spots of high electric field accompanied by strong absorption and scattering which can be observed in three modes: angle resolved mode, wavelength shift and field enhancement imaging mode (Figure 3A-3C), as well as following several other optical properties [8].

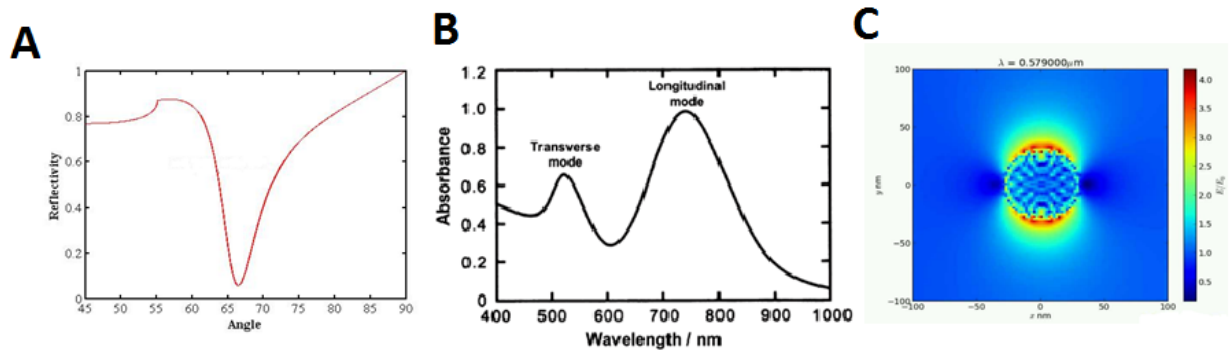

Figure 3. *The three universal mode of observation of the plasmon excitation: (A) angle resolved mode, (B) wavelength shift and (C) field enhancement imaging mode. Reprinted from reference* 8.

Plasmon in noble metals gave birth to plasmonics which is a branch of Nanophotonics that studies how the electromagnetic field can be confined over a dimension of the order or smaller than the wavelength [1, 3]. Applications related to plasmon in AuNPs are impressively tremendous, ranging from sensing to photothermal therapy to cell imaging. In addition, plasmon-enhanced phenomena, including for instance, Raman spectroscopy of metal nearby analytes, catalysis, solar energy conversion are highly impressive for multiple purposes. Furthermore, plasmon excitation is involved in several useful fundamental advanced physical processes such as nonlinear optics, optical trapping, magneto-plasmonics, and optical activity [1, 3, 7, 9].

3. Localized surface plasmon and anisotropy of nanoparticles

LSPR is strongly dependent on sizes, shapes, materials and even the surrounding medium [8]. Metallic nanoparticles of differentsizes and shapes show different absorption properties and thus may display different colors, such as is seen for nanospheres, nanorods and bipyramids (Figures 4A-4G). The anisotropic of nanoparticles is characterized by their aspect ratio which is the length over the width for nanorods and bipyramids [10]. LSPR excitation on an ensemble or bulk sample of isotropic nanoparticles such as nanosphere and nanocube arises in a one resonant mode, however, anisotropic nanoparticles such as nanorods and bipyramids exhibit

two resonant modes, the less polarizable but high energy transverse mode and the highly polarizable with low energy longitudinal mode[11].

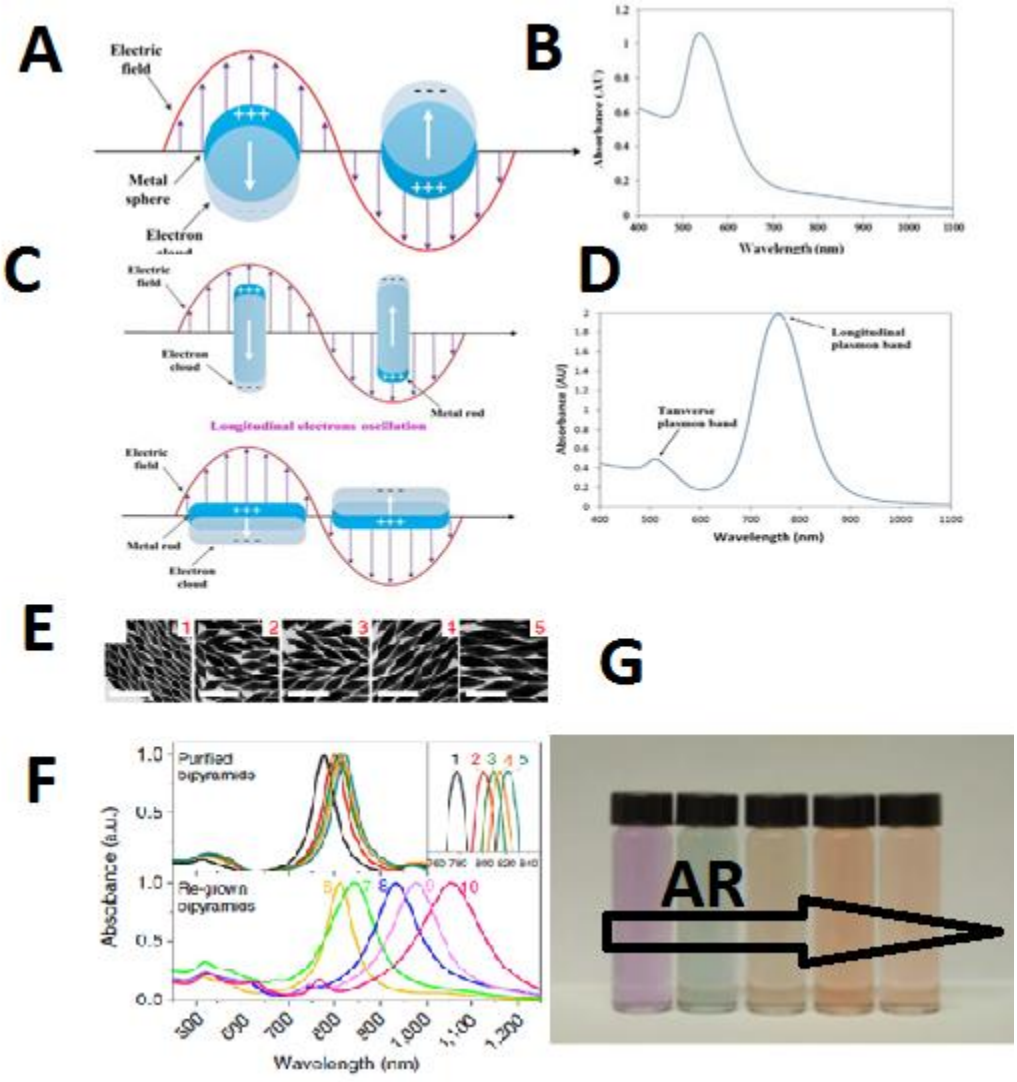

Figure 4. *The illustration of LSPR excitation in relationship with the anisotropic nanoparticles. (A-B) Nanosphere, (C-D) Nanorods and (E-F) Bipyramids. (G) Colors of nanorods colloids as function of aspect ratio. Reprinted from reference 12 and 13.*

4. Localized surface plasmon and Sensing the shapes and the environment of nanoparticles

The ability to monitor LSPR spectral characteristics at the ensemble and single nanoparticle levels has revealed that they are strongly dependent on the geometry, composition, and size of the nanoparticles (Figure 5A) [14, 15] as well as on their local environment (Figure 5B) [16]. Control of these parameters has opened an unprecedented possibility of tuning plasmonic properties and engineering of light.

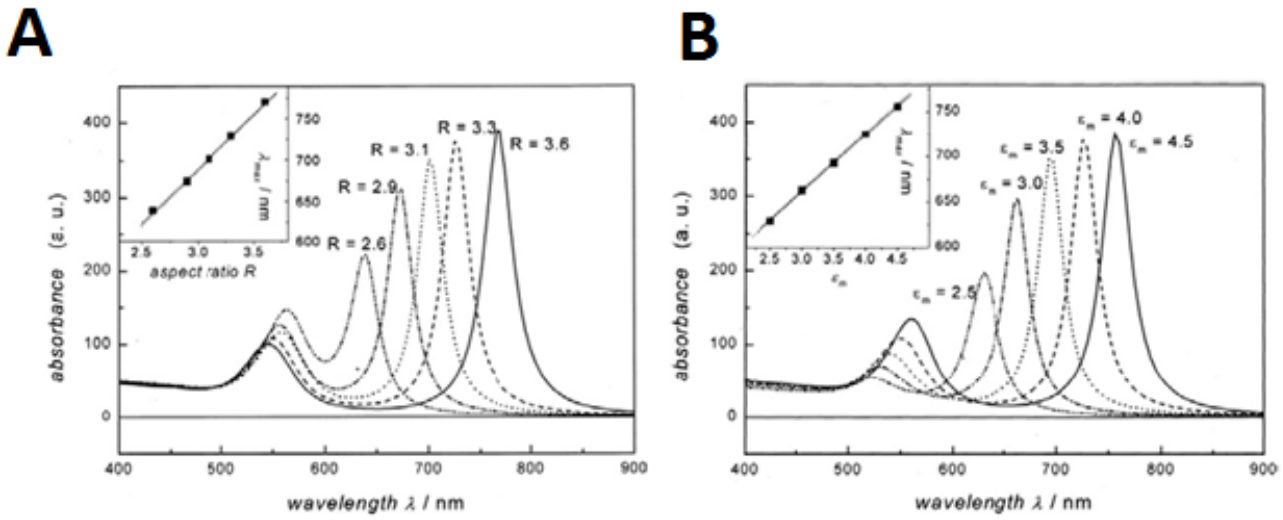

Figure 4. *The redshift illustration of LSPR with the increase of aspect ratio as well as the increase of the local refractive index. Reprinted from reference 12.*

Generally, changes in resonance peaks result in a red shift as well as a broadening of peaks when the size of the nanoparticles or the local RI increases [17]. The local nature RI sensitivity of LSPR has led to the development of nanoparticles as chemo- and biosensors [18]. LSPR sensing the refractive indices has been widely used. In that case the sensitivity is expressed as resonance shift over refractive index (RI) change:

$$Sensitivity = \frac{\Delta\lambda}{\Delta\eta} \qquad \text{(nm/RIU) or (eV/RIU).}$$

Fundamentally, LSPR sensors consist of functionalized particles with target molecule receptors, which LSPR shifts, dampens, or enhances in the presence of target molecules [19]. These changes in nanoparticle optical properties signal the presence of target molecules [20] and facilitate monitoring LSPR by relying on the shift of the peak maximum, the intensity, and broadening of the peaks [21]. Broadening arises from LSPR decay, also known as the damping or dephasing time through energy conversion or energy transfer [11, 23].

5. Averaging and Homogeneous LSPR with the anisotropy of nanoparticles

In contrast to the ensemble sample of isotropic nanoparticles, in a single nanoparticles, only the highly polarizable longitudinal mode has a high probability of occurring with a sharp shape for anisotropic with sharp tips such as bipyramids (Figure 5) [24]. Indeed, for chemically synthesized ensemble nanoparticles, the inherent inhomogeneity or polydispersity (distribution of size and shape). Provide spectral information with hidden (average) or heterogeneous properties of individual nanoparticles [22]. Tremendous advances in experimental techniques and computational modeling, with their relative efficiencies have permitted and facilitated overcoming this limitation on measuring average properties [25]. Therefore, with the measuring of homogeneous properties, LSPR investigation through various scattering/absorption/extinction-based single nanoparticle spectroscopy techniques is growing exponentially and gaining more attention [26], especially for anisotropic single nanoparticles with high polarizability such as gold bipyramids (AuBPs) [27]. Moreover, the ability to monitor LSPR spectral characteristics at the ensemble and single nanoparticle levels has revealed and confirmed that they are strongly dependent on the geometry, composition, and size of the nanoparticles [15, 28] as well as on their local environment [16, 29]. Control of these parameters has opened an unprecedented possibility of tuning plasmonic properties and engineering of light.

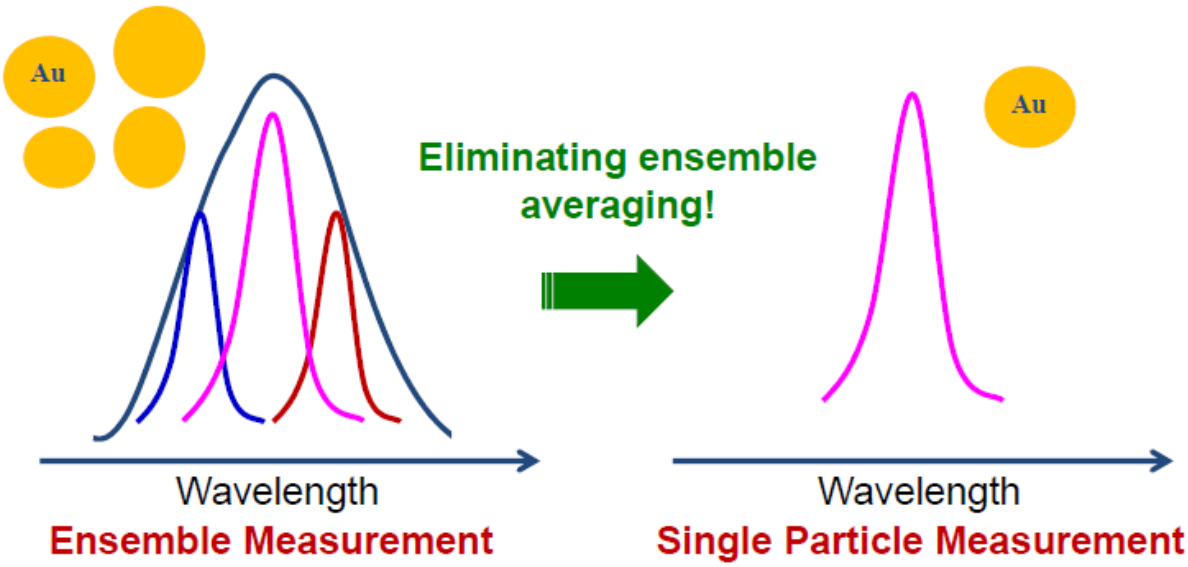

Figure 5. *The averaging effect on the nanoparticles spectra. Reprinted from reference 30.*

6. Single nanoparticles spectroscopy and microscopy in a dark field

Bright-field (BF) microscopy is the most known and simplest type of optical microscopy. BF microscopy relies on transmitted light for illumination of the sample. The objects that strongly absorb light will appear as dark spots on a bright, non-absorbing background. However, the major limitation is low contrast for weakly absorbing samples including biological samples. To overcome this limitation, it is usually required to stain biological samples in order to achieve better contrast under a BF microscope [30, 31]. Besides, another microscopic technique, dark-field (DF) microscopy which the schematic configuration of DF microscopy is shown in Figure 6 is was used in this our investigations. In DF microscopy, the numerical aperture of the condenser is larger than that of the objective. In addition, there is an annular stop in the condenser which blocks the central part of the illumination light beam coming from the base of the microscope. When there is no sample on the microscope stage, the entire field of view appears dark. When a sample is placed on the stage, the scattered light from the sample is collected by the objective lens. In the DF image, the structures of the sample appear bright against the dark background. DF

microscopy allows low contrast samples in BF microscopy to be detected with good signal-to-noise ratios [30-32].

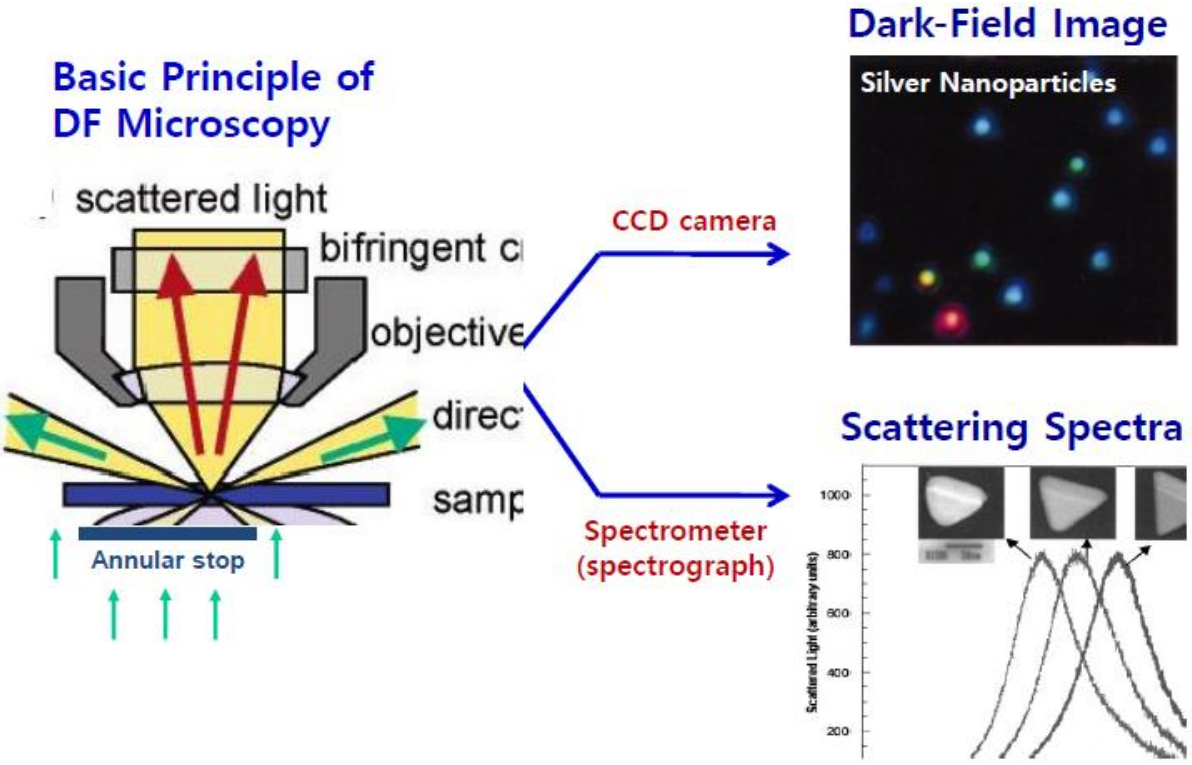

Figure 6. *The working principle of dark-field microscopy and spectroscopy for single nanoparticles studies. Reprinted from reference 32.*

7. Localized surface plasmon resonance mechanisms in gold nanoparticles.

As abovementioned, plasmon excitation is due to the collective motion of hot electron generated by interaction of the material and light, and which lead to the formation of hot spots (high field regions). The plasmon excitation and decay is well described by the Fermi model (Figure 7), in which after excitation plasmon can decay radiatively (Figure 7A) or non-radiatively (Figure 7B-7D) depending the dephasing time [33]. In chemistry we are taught to understand the basic of photophysics in terms of separable electronic and vibrational motions, and excited state dynamics that can be described in terms of radiative and non-radiative decay (or relaxation) processes, such as intersystem crossing and internal conversion. This zeroth-order

picture is helpful for understanding the photo-physical properties of semiconductor nanoparticles, with additional effects such as surface recombination of the charge carriers. However, it breaks down for metal nanostructures. This is because of the high density of empty electronic states at the Fermi level for metals. For metals the starting point for discussing spectroscopy is Mie and related theories [34], which describes the optical response of a spherical particle. Mie theory requires the dielectric constants of the particle and the surroundings as input parameters. The dielectric constants of metals are strongly frequency dependent and contain both real and imaginary components [35]. Roughly, the real part determines the position of the LSPR, and the imaginary part determines the dephasing [22]. Understanding the frequency dependent of dielectric not only permit to get a deep insight on the theory behind the absorption of photons by a metal nanoparticle, and the subsequent energy relaxation processes, as well as LSPR mechanism is hidden in the optical signal characteristics [22, 34].

The energy stored in the elevated LSPR fields (hot spots) is dissipated either through radiative (Figure 7A) photon scattering or non-radiative (7B-7D) absorption in the metal nanoparticles within a very short time period, as the lifetime of a plasmonic excitation is in the femtosecond range [33].

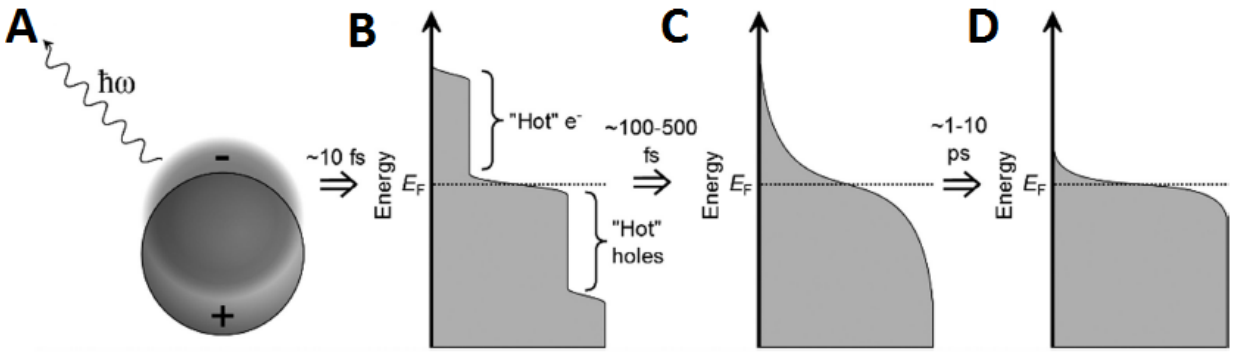

Figure 7. *Illustration of the plasmonic decay process. (a) Radiative decay of the Plasmon. Non-radiative decay processes including (b) dephasing into energetic electrons and holes, (c) thermalization of hot carriers, and (d) relaxation of hot carriers into phonons. Reprinted from reference 33.*

Non-radiative absorption results in the generation of energetic charge carriers in the metal nanoparticles. Absorption (that is, the generation of energetic charge carriers) in metals can occur through either intraband s-to-s excitations or interband d-to-s excitations (Figure 8).

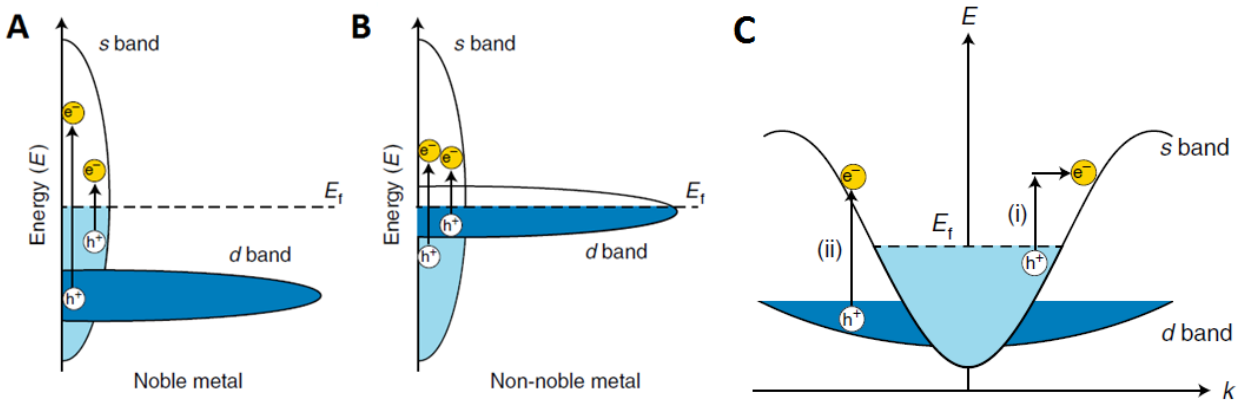

Figure 8. *(A) (B), Sketches of the density of states of a plasmonic metal (A) and non-noble transition metal (B). Intraband s-to-s transitions are accessible with visible light photons for all metals. As the d band lies far before the Fermi level (Ef) for plasmonic metals, only high-energy photons can induce interband d-to-s excitations for these metals. In the case ofnon-noble metals, the d band intersects the Fermi level allowing for d-to-s excitations to take place throughout the visible range. Band diagram (energy (E) versus momentum (k)) depiction of photon absorption in metals through either s-to-s intraband excitations (i) or d-to-s interband excitations (ii). Intraband excitations require a change in momentum whereas interband excitations are direct electronic excitations, which do not require a change in momentum. Reprinted from reference 36.*

Due to the inherently larger rate constant of interband excitations (Figure 8ii), plasmon decay via these excitations is the dominant decay pathway when available. Recent first principles calculations showed by the partitioning among various absorption pathways in plasmonic gold nanoparticles versus plasmon (photon) energy for different particle sizes. The data showed that direct interband

excitations are the dominant pathway for plasmon decay (photon absorption) in Au nanoparticles at energies where they are energetically accessible regardless of nanoparticle size. The contribution of the other absorption processes (that is, the phonon assisted or surface-assisted intraband s-to-s excitations) are size dependent and only dominate for plasmon energies at which direct interband transitions are inaccessible [36]. In noble metals, two transitions (Figures 7), that is intraband ((Figure 8i) and interband (Figure 8ii) can be distinguish giving rise to two most known frequency dependent dielectric models (Figures 9A-9B) [37].

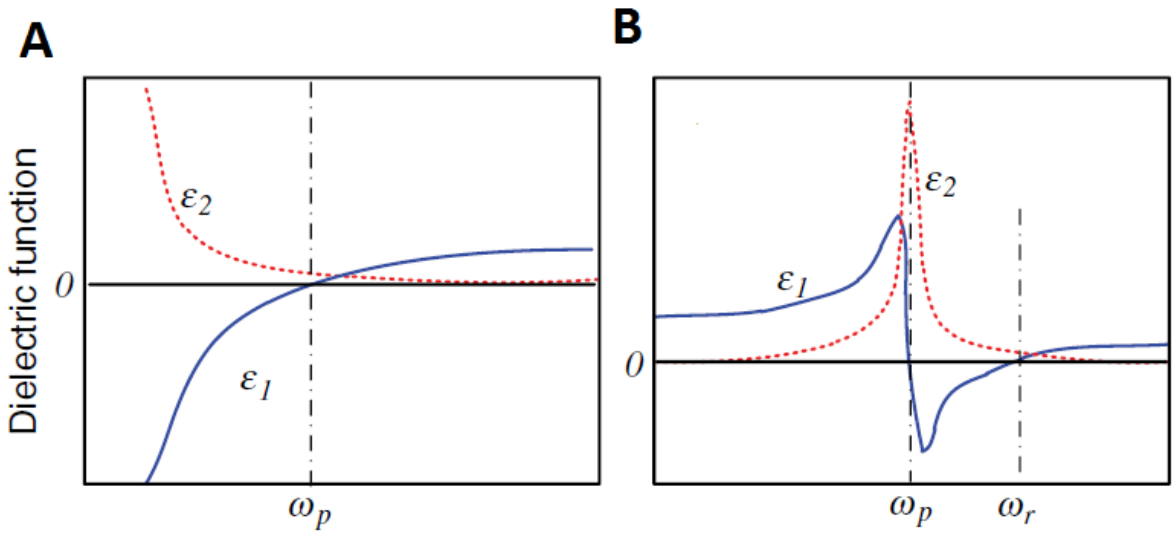

Figure 9. *Components of the complex dielectric functions for (a) metals described using the Drude model and (b) dielectrics using the Lorentz equations. Reprinted from reference 37.*

The simplest realistic model for the dielectric constant of a metal is the Drude or free electron model (Figure 7A), which was developed to describe DC conductivity. For many metals, this model gives reasonable results up to optical frequencies, with suitable modifications because of interband transitions. For noble metals like Ag and Au, the Drude model gives a good description of the dielectric constants in the near-IR region of the spectrum, but it breaks down in the visible to near-UV region because of interband transitions. The onset of the interband transitions is at ca. 2.4 eV for Au, and 3.9 eV for Ag [34].

The frequency and size dependence of the dielectric function of gold affects the plasmon linewidth due to the bulk damping contribution [38]. The dielectric function of gold is frequency and size dependent and a complex function (Eq. S5).

$$\tilde{\varepsilon}(\omega, size) = \varepsilon_r + i\varepsilon_i \quad \text{(S5)}$$

For metals, the most realistic expression that account intraband and interband electronic transition for the CDF is dependent on the size and shape of AuNPs included as contributions in the LSPR damping Γ (bulk ($\Gamma_{bulk} \sim v_F / l_\infty$, v_F: Fermi velocity, l_∞: bulk mean free path of electrons between two collisions), radiation ($\Gamma_{rad} = 2\pi\hbar\kappa_{rad}V$, K_{rad}: proportionality constant, V: particle volume) and surface scattering ($\Gamma_{surf} = A_{surf} v_F / l_{eff}$, A_{surf}: proportionality constant that describe the probability that an electron scattered at the particle surface, l_{eff}: effective mean free path length of electrons which gives the average distance an electron needs to travel before reaching a surface)) [8,40-41]. That is, when the size becomes comparable or smaller than the bulk mean free path l_∞ of the metal free electrons between collisions, the damping increase as additional scattering effective mean free path l_{eff} of the conduction electrons from the surface give rise to Γ_{surf}. In case of smaller sizes than the bulk, the volume (V) become smaller and the radiation (Γ_{rad}) contribution become negligible [22, 38]. Another contribution is omitted here that arises due to the chemical effect at the interface of gold nanoparticles, which is known as chemical interface damping (CID) Γ_{CID} [22].

8. References

1. V. Amendola, R. Pilot, M. Frasconi, O. M. Marago and M. A. Iati, *Journal of physics. Condensed matter: an Institute of Physics journal*, 2017, 29, 203002.

2. P. Mulvaney, *Langmuir*, 1996, 12, 788-800.

3. S. Link, D.J. Masiello, Chem. Rev. 2018, 118, 2863-2864.

4. L.-Y. Hsu, W. Ding and G. C. Schatz, *The Journal of Physical Chemistry Letters*, 2017, 8, 2357-2367.

5. K. D. Chapkin, L. Bursi, G. J. Stec, A. Lauchner, N. J. Hogan, Y. Cui, P. Nordlander and N. J. Halas, *Proceedings of the National Academy of Sciences*, 2018.

6. K.A.Willets, R.P. Van Duyne. Localized surface plasmon resonance spectroscopy and sensing, *Annu Rev Phys Chem.* 2007;58:267-97.

7. O. Schnitzer, V. Giannini, S. A. Maier and R. V. Craster, *Proceedings of the Royal Society A: Mathematical, Physical and Engineering Science*, 2016, 472.

8. P. V. Tsalu, G. W. Kim, J. W. Hong and J. W. Ha, *Nanoscale*, 2018, 10, 12554-12563.

9. Liang-Yan Hsu, Wendu Ding, and George C. Schatz, *The Journal of Physical Chemistry Letters* 2017, 10, 2357-2367

10. S. W. Moon,P. V. Tsalu and J. W. Ha, *Phys. Chem. Chem. Phys.,* 2018,20, 22197-22202

11. Bok, H. M.; Shuford, K. L.; Kim, S.; Kim, S. K.; Park, S., Multiple surface plasmon modes for gold/silver alloy nanorods. *Langmuir : the ACS journal of surfaces and colloids* **2009,***25* (9), 5266-70.

12. J. Cao, T. Sun and K. T. V. Grattan, *Sensors and Actuators B: Chemical*, 2014, 195, 332-351.

13. J.-H. Lee, K. J. Gibson, G. Chen and Y. Weizmann, *Nature Communications*, 2015, 6, 7571.

14. Derkachova, A.; Kolwas, K.; Demchenko, I., Dielectric Function for Gold in Plasmonics Applications: Size Dependence of Plasmon Resonance Frequencies and Damping Rates for Nanospheres. *Plasmonics (Norwell, Mass.)* **2016,***11*, 941-951.

15. Nehl, C. L.; Hafner, J. H., Shape-dependent plasmon resonances of gold nanoparticles. *Journal of Materials Chemistry* **2008,***18* (21), 2415-2419.

16. Ringe, E.; M. McMahon, J.; Sohn, K.; Cobley, C.; Xia, Y.; Huang, J.; C. Schatz, G.; D. Marks, L.; P. Van Duyne, R., Unraveling the Effects of Size, Composition, and Substrate on the Localized Surface Plasmon Resonance Frequencies of Gold and Silver Nanocubes: *A Systematic SingleParticle Approach*. 2010; Vol. 114, p 12511-12516.

17. Wang, Y.; Tang, L., Chemisorption Assembly of Au Nanorods on Mercaptosilanized Glass Substrate for Label-free Nanoplasmon Biochip. *Analytica chimica acta* **2013,***796*, 10.1016/j.aca.2013.08.024.

18. Soares, L.; Csaki, A.; Jatschka, J.; Fritzsche, W.; Flores, O.; Franco, R.; Pereira, E., Localized surface plasmon resonance (LSPR) biosensing using gold nanotriangles: detection of DNA hybridization events at room temperature. *Analyst* **2014,***139* (19), 4964-4973.

19. Nusz, G. J.; Curry, A. C.; Marinakos, S. M.; Wax, A.; Chilkoti, A., Rational Selection of Gold Nanorod Geometry for Label-Free Plasmonic Biosensors. *ACS nano* **2009,***3* (4), 795-806.

20. Hu, M.; Novo, C.; Funston, A.; Wang, H.; Staleva, H.; Zou, S.; Mulvaney, P.; Xia, Y.; Hartland, G. V., Dark-field microscopy studies of single metal nanoparticles: understanding the factors that influence the linewidth of the localized surface plasmon resonance. *Journal of materials chemistry* **2008,***18* (17), 1949-1960.

21. Yang, S.; Wu, T.; Zhao, X.; Li, X.; Tan, W., The Optical Property of Core-Shell Nanosensors and Detection of Atrazine Based on Localized Surface Plasmon Resonance (LSPR) Sensing. *Sensors (Basel, Switzerland)* **2014,***14* (7), 13273-13284.

22. Olson, J.; Dominguez-Medina, S.; Hoggard, A.; Wang, L.-Y.; Chang, W.-S.; Link, S., Optical Characterization of Single Plasmonic Nanoparticles. *Chemical Society reviews* **2015,***44* (1), 40-57.

23. Otte, M. A.; Sepulveda, B., Figures of Merit for Refractometric LSPR Biosensing. In *Nanoplasmonic Sensors*, Dmitriev, A., Ed. Springer New York: New York, NY, 2012; pp 317-331.

24. Schneider, T.; Jahr, N.; Jatschka, J.; Csaki, A.; Stranik, O.; Fritzsche, W., Localized surface plasmon resonance (LSPR) study of DNA hybridization at single nanoparticle transducers. *Journal of Nanoparticle Research* **2013,***15* (4), 1531.

25. Ringe, E.; Sharma, B.; Henry, A.-I.; Marks, L. D.; Van Duyne, R. P., Single nanoparticle plasmonics. *Physical Chemistry Chemical Physics* **2013,***15* (12), 4110-4129.

26. Kleinman, S. L.; Bingham, J. M.; Henry, A.-I.; Wustholz, K. L.; Duyne, R. P. V. In Structural and optical characterization of single nanoparticles and single molecule SERS, SPIE NanoScience + Engineering, SPIE: 2010; p 10.

27. Li, Q.; Zhuo, X.; Li, S.; Ruan, Q.; Xu, Q.-H.; Wang, J., Production of Monodisperse Gold Nanobipyramids with Number Percentages Approaching

100% and Evaluation of Their Plasmonic Properties. *Advanced Optical Materials* **2015,***3* (6), 801-812.

28. Derkachova, A.; Kolwas, K.; Demchenko, I., Dielectric Function for Gold in Plasmonics Applications: Size Dependence of Plasmon Resonance Frequencies and Damping Rates for Nanospheres. *Plasmonics (Norwell, Mass.)* **2016,***11*, 941-951.

29. Ha, JW. Special topics of analytical chemistry, 2018, cours materials.

30. Ha, Ji Won, "Single Molecule and Nanoparticle Imaging in Biophysical, Surface, and Photocatalysis Studies". Graduate Thesesand Dissertations, 2013. 13494.

31. Anthony S. Stender, Kyle Marchuk, Chang Liu, Suzanne Sander, Matthew W. Meyer, Emily A. Smith, Bhanu Neupane, Gufeng Wang, Junjie Li, Ji-Xin Cheng, Bo Huang, and Ning Fang, Chemical Reviews 2013 113 (4), 2469-2527

32. Carsten Sönnichsen and and A. Paul Alivisatos, Nano Letters 2005 5 (2), 301-304.

33. Rebecca L. Gieseking, Mark A. Ratner, and George C. Schatz, Frontiers of Plasmon Enhanced Spectroscopy Volume 1. January 1, 2016 , 1-22

34. Gregory V. Hartland. Chemical Reviews 2011 111 (6), 3858-3887

35. Ashcroft, N. W.; Mermin, N. D. Solid State Physics; Holt, Rinehart & Winston: New York, 1976.

36. U. Aslam, V. G. Rao, S. Chavez and S. Linic, Nature Catalysis, 2018, 1, 656-665.

37. Yongqian Li. Plasmonic Optics: Theory and Applications, 2017, https://doi.org/10.1117/3.2263757.ch1.

38. B. Foerster, A. Joplin, K. Kaefer, S. Celiksoy, S. Link and C. Sönnichsen, *ACS Nano*, 2017, 11, 2886-2893.

39. A. Derkachova, K. Kolwas and I. Demchenko, *Plasmonics*, 2016, 11, 941-951.

40. J. Lermé, H. Baida, C. Bonnet, M. Broyer, E. Cottancin, A. Crut, P. Maioli, N. Del Fatti, F. Vallée and M. Pellarin, *The Journal of Physical Chemistry Letters*, 2010, 1, 2922-2928.

41. A. Alabastri, S. Tuccio, A. Giugni, A. Toma, C. Liberale, G. Das, F. De Angelis, E. Di Fabrizio and R. P. Zaccaria, *Materials*, 2013, 6, 4879-4910.

CHAPTER 3:

HOMOGENEOUS LOCALIZED SURFACE PLASMON RESONANCE INFLECTION POINTS FOR ENHANCED SENSITIVITY AND TRACKING PLASMON DAMPING IN SINGLE GOLD BIPYRAMIDS

Philippe Vuka Tsalu, Geun Wan Kim, and Ji Won Ha*

A paper published in *Nanoscale,* **2018, 10, 12554-12563**.
Reproduced by permission of the Royal Society of Chemistry (RSC)
* Corresponding author

Abstract

The most polarizable localized surface plasmon resonance (LSPR) longitudinal mode of anisotropic metallic nanoparticles, such as gold bipyramids (AuBPs),is of high prominence. This optical response has tremendous applications from spectroscopy to photonics and energy devices to sensing. In conventional gold LSPR-based sensing, broadening and asymmetry in peaks due to chemical and instrument noise hinder obtaining a precise insight on shift positions, accordingly limiting the effectiveness and impact of LSPR sensors. Further, when investigating LSPR properties, utilizing more simplistic frequency dependent dielectric-type models can aberrantly impact the reliability of fundamental properties used for designing and fabricating efficient optical devices. For instance, more approximations can effectively limit screening intra-band and inter-band electronic (IB) transition contributions and other related optical properties. With an aim to find alternative methods to further improve their efficiency, as a first report, we devoted a particular focus on LSPR scattering inflection points (IFs) of single gold bipyramids (AuBPs). The findings reveal that tracking LSPR IFs exhibit high sensitivity over their counterpart LSPR peak shift locations. In addition, we newly detected IB transition contributions near the resonance energy in the range (1.50 eV~2.00 eV) dominated by intra-band transitions. A small increase in the local RI effectively enhances the

LSPR quality factor due to IB transitions. Thus, while neglecting IB transitions in the range below 2.4 eV can work for local air RI, in high local RI media it can be aberrantly underestimated. Demonstrated by the use of the dielectric function based on Kramers-Kronig consistent Lorentz oscillators, our findings are in good agreement with the enhancing RI sensitivity effect. The results of this investigation support the idea that tracking curvature changes of an optical signal can be effectively used for LSPR longitudinal peak energy RI sensing as well as damping in the local RI environment of a single AuBP.

Introduction

The plasmonic effect associated with localized surface plasmon resonance (LSPR) and excited by an impinged oscillating electromagnetic radiation on noble metal nanoparticles under the quasi static approximation condition is regarded as involving collective or coherent oscillations of the conduction band electrons of nanoparticles[1,2]. Under these subwavelength structure conditions, not only are electrons polarized and resonate, but the local electromagnetic field is enhanced. The strong interaction of metal nanoparticles with the incident electromagnetic field causes light to be confined to sub-diffraction volumes and optical absorption/scattering of a selective photon energy to be effectively enabled[3,4]. Over many years, LSPR has been intensively investigated, which has permitted the optical properties of nanoparticles to be monitored by conventional UV-Visible spectroscopy and far-field techniques[5]. Currently, LSPR has a variety of applications ranging from spectroscopy[6], such as surface enhanced Raman spectroscopy [7] (SERS); to sensing[8], for instance plasmon-enhanced fluorescence[9], SERS[10] and other techniques, and energy devices[11] as plasmonic solar cells[12]; to photonics[13,14] for example nanoscale lasers[15] and metamaterials[16]. More importantly, the particular case of gold nanoparticles (AuNPs), relative to other metallic nanoparticles has attracted considerable attention because of their intrinsic or unique properties[17], biocompatibility[18] due to high chemical and physical stability[19], large numbers of easily polarizable conduction electrons[20] for preferential interaction with an electromagnetic field[21] and generation of nonlinear optical phenomena[22], easy surface modification or functionalization[23] with organic and biological molecules[24], and a

multitude of optical properties[25] related to surface modification and their environment in spectroscopy and sensing experiments. Therefore, this broad range of advantages and applications has stimulated and fostered their use in bio and chemical LSPR based sensors[26,27].

In addition, LSPR excitation on an ensemble or bulk sample of anisotropic AuNPs exhibits two resonant modes, the less polarizable but high energy transverse mode and the highly polarizable with low energy longitudinal mode[28]. In contrast, with a single AuNP, only the highly polarizable longitudinal mode has a high probability of occuring.[29] Indeed, for chemically synthesized ensemble nanoparticles, the inherent inhomogeneity or polydispersity (distribution of size and shape) provide spectral information with hidden (average) or heterogeneous properties of individual nanoparticles[20]. Tremendous advances in experimental techniques and computational modeling, with their relative efficiencies have permitted and facilitated overcoming this limitation on measuring average properties[30]. Therefore, with the measuring of homogeneous properties, LSPR investigation through various scattering/absorption/extinction-based single nanoparticle spectroscopy techniques is growing exponentially and gaining more attention[31], especially for anisotropic single nanoparticles with high polarizability such as gold bipyramids (AuBPs)[32].

Moreover, the ability to monitor LSPR spectral characteristics at the ensemble and single nanoparticle levels has revealed that they are strongly dependent on the geometry, composition, and size of the nanoparticles[33,34] as well as on their local environment[35]. Control of these parameters has opened an unprecedented possibility of tuning plasmonic properties and engineering of light. Generally, changes in resonance peaks result in a red shift as well as a broadening of peaks when the size of the nanoparticles or the local RI increases[36].The local nature RI sensitivity of LSPR has led to the development of nanoparticles as chemo- and biosensors[37]. Fundamentally, LSPR sensors consist of functionalized particles with target molecule receptors, which LSPR shifts, dampens, or enhances in the presence of target molecules[38].These changes in nanoparticle optical properties signal the presence of target molecules[39] and facilitate monitoring LSPR by relying on the shift

of the peak maximum, the intensity, and broadening of the peaks[40]. Broadening arises from LSPR decay, also known as the damping or dephasing time through energy conversion or energy transfer[20, 41].

Although researchers have taken advantage of all of these tremendous applications, LSPR still has many fundamental limitations that cause LSPR based sensor efficiency to be low compared to surface plasmon polariton (SPP) sensors[42]. In AuNPs, the LSPR related optical properties accuracy determination are impacted by a realistic representation of the frequency dependent dielectric function of the nanoparticles[43]. Therefore, simplistic models negatively impact the fundamental quantities that are necessary for the design and fabrication of reliable devices based on plasmonic resonances[44]. A realistic representation of the frequency dependent dielectric function consists of intra-band and inter-band electronic (IB) transitions. The former account for free carriers, whereas the latter account for bound electrons[45]. Because for metals, free carriers dominate, Drude-type models were reliably used to describe material properties for silver. However, applying this model to AuNPs does not work perfectly above a threshold where IB transitions should be corrected[46]. In the visible and near infrared, 2.4 eV is the most used threshold to ignore the effect of IB transitions on gold plasmons[44, 47]. Whereas in the same frequency range, Derkachova et al. reported 1.8 eV to be the threshold according to their experimental findings[43]. In attempting to correct IB transition contributions by use of the Lorentz bound electron model, Alabastri et al. showed that the threshold can vary depending on the resonance location[44]. In the literature, there are no studies that quantitatively provide IB transition contributions to the frequency range dominated by intra-band electronic transitions due to free carriers.

One other major limitation of LSPR sensor effectiveness is changes in the magnitude of the shift across the spectrum due to the shape of the LSPR peak when monitoring changes of the nanoparticle local environment at their surface[48]. This results in unsymmetrical broadening and was found to have a negative impact on sensing efficiency[49].Methods such as lithography have been attempted to improve efficiency, but they tended to be high cost, low yielding, and tedious to process[42]. Recently P. Chen et al. theoretically attempted to use Mie theory to evaluate LSPR

curvature changes on ensemble samples with respect to RI changes. They developed an analytical expression as a function of RI and operated second derivatives to obtain the curvature for various values of RI[42]. In a second report, they demonstrated that inflection points at the long wavelength side of the LSPR extinction spectrum peak maximum of ensemble samples show better RI sensitivity[48]. However, other than sensitivity, they did not provide quantitatively any other optical information on energy transfer such as broadening. Their report was limited to only ensemble samples of nanoparticles rather than single particles. Moreover, we are not aware of any additional reports of inflection points on single nanoparticles as well as their broadening effect.

For further improvement of the performance of LSPR assays and accordingly LSPR sensors, it is reasonable to gain insight into all of the aforementioned limitations. As part of our effort, in this first report, we used a facile method to obtain LSPR inflection points of experimentally determined LSPR scattering. We then investigated both LSPR response damping and sensing effects on the local vicinity of single AuBPs embedded in three local RI media (air, water, and oil) suspended on a SiO_2 glass slide substrate. In addition, homogeneous scattering spectra with a Kramers-Kronig consistent Lorentz oscillator permitted us to derive IB transition contributions in the frequency range near the LSPR excitations where intra-band electronic transitions dominate. RI sensitivity from changes of the derived analytical complex dielectric functions in the neighborhood of single AuBPs was also investigated.

Experimental Section

Materials and Sample Preparation

AuBPs used in this study were synthesized via a seed-mediated method. The average width and length of AuBPs were determined to be 26 nm and 76 nm, respectively. The samples were prepared as follows. Briefly, the colloid solution was first diluted with 18.2-MΩ pure water to a proper concentration. The diluted solution was then sonicated for 10 min at room temperature. Samples were prepared by spin casting on pre-cleaned SiO2 glass slides. Then, a 22 mm x 22 mm No. 1.5 coverslip

(Corning. NY) was placed on the glass slide. Although AuBPs in the water refractive index samples were used directly, to obtain air and oil refractive indexes, samples were dried at room temperature, which permitted a change from the air refractive index medium to oil. Throughout all of the experiments, the concentration of AuBPs on the glass slide surface was controlled to be approximately 1 μm-2 in order to facilitate single particle characterization and to minimize inter-particle SPR coupling resulting in spectral shifts.

Characterization of Gold Bipyramids

To ensure the shapes and dimensions, structural characterization of AuBPs was performed using scanning electron microscopy (SEM). Figure S1A illustrates the shape of AuBPs in a SEM image. Further, heterogeneous LSPR ensemble absorption spectra in water were recorded with a Varian Carry 100 UV-Vis spectrometer. The high energy transverse and low energy longitudinal absorptions are depicted in Figure S1B.

Single Particle Microscopy and Spectroscopy

In a dark home-built system, dark-field (DF) microscopy imaging was carried out under a Nikon inverted microscope (ECLIPSE Ti-U). In DF mode, the microscope utilized a Nikon Plan Fluor 100x 0.5-1.3 oil iris objective and a Nikon DF condenser. An Andor iXon EM+ CCD camera (iXon Ultra 897) was employed to record DF images of AuBPs. The collected images were analyzed with the Image J software. Furthermore, DF scattering spectra were acquired with an Andor spectrophotometer (SHAMROCK 303i, SR-303I-A) and an Andor CCD camera (Newton DU920P-OE). When obtaining a spectrum, the scanning stage moved the sample to the desired location so that only scattered light from the selected location was collected by the objective. The scattered light was directed to the entrance of the spectrophotometer, dispersed by a grating (300 l/mm, center wavelength of 700 nm), and detected by the Newton CCD camera. The background was measured at a region without any particles. Data analysis was performed with specially designed Matlab programs.

Results and Discussion

AuBPs with the average size of 26 nm · 76 nm were used and synthesized via a seed-mediated method. In the present study, resonance energy and damping factor (E_o and Γ) were inferred by the use of LSPR scattering intensities of single AuBPs obtained by the far-field technique dark-field (DF) microscopy and spectroscopy. Figures 1A and 1B show a DF image and single spectrum of a AuBP1embedded in water. As shown in Figure 1B, scattering spectrum of single AuBP1 was well fitted with a Lorentzian function. More single particle spectra in various RI media are given in the Supporting Information (Figures S2A, S3A, and S4A). In Figure S1B illustrating an ensemble absorption spectrum of AuBPs dispersed in water, while the transverse LSPR peak with high energy appears at approximately 516 nm (2.40 eV), the longitudinal LSPR peak with low energy is located at around 735 nm (1.69 eV). A single sharp peak is located at 721 nm (1.72 eV)in Figure 1B corresponding to longitudinal plasmon resonance, which is consistent with the ensemble spectrum in Figure 1B. The high energy transverse LSPR peak is not observed, which is in good agreement according to the characteristics of a single AuBP[50].

Unlike the study of P. Chen et al., to perform first and second derivatives of our experimental LSPR scattering spectra, a facile method that uses the Lorentzian fitting curve function form (EquationsS3, S5, and S6)related to the scattering cross-section from Mie theory including only the dipolar mode for ellipsoids(Equations S1 and S2) was performed[20]. The first, second, and third rows shown in Figures 2A-2C represent the LSPR scattering spectra (Figures S2A-S2B, Figures S3A-S3B and Figures S4A-S4B for full details) and the corresponding first (Figures S2C, S3C, and S4C for full details) and second order derivatives (Figures S2D, S3D and S4D for full details), respectively. Unlike the rows, the columns are differentiated by three colors corresponding to the local RI media used; the red, blue, and green colors correspond to local air, water, and oil RI, respectively. The LSPR scattering peak maxima in the three local RI media, depicted by a capital B, are located at values 1.90 eV, 1.72 eV, and 1.56 eV for local air, water, and oil RI media, respectively, whereas the local maxima and minima of the first order derivatives

flanking the LSPR peak maxima (B) are represented by A/C, situated at values 1.85 eV/1.95 eV, 1.68 eV/1.75 eV and 1.54 eV/1.59 eV for local air, water, and oil RI media, respectively. Accordingly, A and C represent also the two IFs, i.e., the 0 values of the second order derivatives spectra. IFs coincide with the local maxima/minima of the first order derivatives and appear at the same points A and C on the photon energy axis for the three local RI media. As seen in the first order derivative, B appears to be the critical point of LSPR scattering spectra, i.e., the 0 values of the first order derivatives of the LSPR scattering spectra.

As described, the characteristics of the shapes of these LSPR scattering spectra first and second order derivatives against the photon energies were consistent with those reported on IFs of LSPR extinction spectra of ensemble samples of gold[48]. In addition, the 0 of the first order derivatives fall exactly at the points B (LSPR peak maxima), the point of symmetry for the three local RI media. We notice by analyzing the curvatures that LSPR scattering curves and second order derivatives are even functions and symmetrical to the intensity axis direction, whereas the first order derivative curves are odd functions and are symmetrical to the photon energy axis. This mathematical characteristics are similar to that of the shape and variation of the real part of the complex polarizability/dielectric function against frequency/energy provided by the dipole approximation IB transition contributions given by the Kramers-Kronig consistent Lorentz model[51]. The real part of the complex dielectric functions (here the first derivatives) determines the plasmon resonance position, whereas the imaginary part (here the second derivatives) governs the linewidth[20]. Changes in the real part and imaginary parts are obtained from Kramers-Kronig transformations[52]. Based on the consistency of these symmetrical properties with the Kramers-Kronig transformations, we derived IB transition contributions by utilization of the LSPR energy peak parameters. This approach permits us to gain insight on IB contributions in the LSPR resonance range below 2.4 eV where intra-band transitions dominate over IB transitions. Furthermore, we use the IB transition contributions to investigate theirs effects by changing the RI in the local vicinity of AuBPs. In analyzing these spectra and their derivative characteristics with the energy values given above for A, B, and C in Figures 2A-2C, shift changes

(red-shifts) of LSPR scattering peaks maxima (B), the local maxima/minima and the IFs (A and C) when changing the local RI around single AuBPs from the shapes of the LSPR peaks and the first and second order derivatives, respectively, can obviously be observed. Measurement of LSPR (B) scattering spectra in multiples of 10 for each local RI index exhibited the same results, which were determined to be 1.82 (±0.05) eV, 1.69 (±0.03) eV and 1.58 (±0.03) eV relatively to local air, water, and oil RI, respectively. Similarly, the IFs were also determined with values of 1.78 (±0.05) eV (A) and 1.86 (±0.05) eV (C), 1.66 (±0.03) eV (A) and 1.73 (±0.03) eV (C), and 1.55 (±0.03) eV (A) and 1.61 (±0.03) eV (C), respectively. Further, given in the regime relevant to sensing properties, that the peak energies are with good approximation linear functions of local RI media[53], we consider A, B, and C peak energies and test their linearity to local air, water, and oil RI media. Figure 2D shows plots of energy peaks A, B, and C against local air, water, and oil RI media with corresponding values equal to 1.00, 1.33, and 1.52, respectively. As seen in Figure 2D, the peak energies A, B, and C linearize with the local RI media. The use of a linear fitting function allowed us to determine the slopes as 0.59 eV·RIU^{-1} (R^2 = 0.9875) for peak A, 0.64 eV·RIU^{-1} (R^2 = 0.9868) for peak B, and 0.70 eV·RIU^{-1} (R^2 = 0.9872) for peak C. It is notable that inflection point C exhibited the highest sensitivity with respect to A and the LSPR peaks maxima (B) as shown in Figure 2F (see Tables S1~S4 for full details). Interestingly, the local RI sensitivity improved by 9.38% with respect to the LSPR peak maximum. This result is consistent with earlier reports with gold ensembles for the use of IFs to improve sensitivity[48]. The present results highlight, however, that in regimes relevant to a sensing experiment, the same method can be applied to the experiment of sensing essays for single scattering nanoparticles with a single resonant mode such as AuBPs.

More importantly, one striking element in the first and second order derivatives that has not been considered in the previous study of P. Chen et al.when comparing them in different local RI media, they broaden to the same extent as the LSPR scattering peaks, as shown by the width distances AC as illustrated by the black and magenta dashed parallel vertical lines (Figures 2A-2C). Indeed, we can readily see from the width distances AC that the increase of local RI medium reduces

the distance AC in energy units or increases it in wavelength units. A decrease in energy units of the AC width corresponds to a decrease in the intensity and broadening of the LSPR peaks. Therefore, the LSPR linewidth, i.e., full width at half maximum (FWHM) of single AuBPs in local air, water, and oil RI media was determined to be 0.143 (±0.020) eV, 0.131 (±0.029) eV and 0.099 (±0.009) eV, respectively. Thus, the increase of local RI has broadened the LSPR scattering to 7.69% for water and 40% for oil. The negligible increase observed on local RI changes has previously been discussed for anisotropic single gold nanorods[54]. To the best of our knowledge, this is the first report to observe the effect with single AuBPs with sharp tips.

Since the optical constants must satisfy Kramers-Kronig transformations to be physically relevant and given the LSPR peak and first order derivative curves are Lorentzian-like, we derived the phase-like changes (Equation S2d) in order to have a deeper insight into the peak broadening behavior in relation to the IFs and IB transitions. Changes in phase are derived against photon energy by the use of LSPR scattering peaks and first derivatives (Figures S2E, S3E, and S4E for full details). We expect to obtain a significant relation between the energy width AC and the sensitivity on the shapes of the LSPR peaks, first and second order derivative curves of the LSPR peaks, accordingly, to obtain better understanding of the high sensitivity of the IF C compared to that of LSPR peak maximum shifts used in traditional sensing experiments. Figure 2F shows the changes of the LSPR phase illustrated in local air RI plotted against photon energy. From the phase changes, we can readily see the location of LSPR energy/resonance frequency at the dephasing energy position and two steady states, the low phase steady state around 0 radians and the high phase steady state around 3 radians (see Figures S2E, S3E and S4E for full details). It is striking that this result is in good agreement with the fundamental theory of plasmon IB transitions. Indeed, it has been reported that at the energy excitation of the plasmon, the electrons oscillate coherently with a phase angle situated between 0 and 3 radians[55]. At the resonance frequency or LSPR, there is quick dephasing from the high phase steady state to the low phase steady state. The analysis of the phase changes plotted against photon energy with the two tangent

points at A and C reveals that on the energy range of the sensitivity of the IFs A and C two phase steady states, suggesting that the sensing of these inflection points is more stable to photon energy changes than the sensing of the LSPR peak maximum (B) located in resonance energy where the phase readily changes. Further, the stability of IFs to sensing effects due to the local RI media can be justified by the small tangent slopes, tan 1 (pink) and tan 2 (black) at A and C on the phase changes.

As mentioned above, we used the Kramers-Kronig transformations consistent with Lorentz oscillators, to derive the changes in the real and imaginary parts with contributions of IB transitions near the resonance/LSPR energies. Figures 3A-3C show the derived frequency-dependent complex dielectric functions change around the ranges of resonant energy of AuBPs embedded in air (red), water (blue), and green (oil) (Figures S5A-5B, S6A-S6B and S7A-S7B for full details). As can be seen inFigures 3A-3C, we successfully derived the IB transition based frequency-dependent dielectric functions in the three local RI media. Indeed, it is obvious at the resonance photon energy ($E=E_o$), $Re[\varepsilon(E_o)] = 1$ and $Im[\varepsilon(E_o)]$ take the maximum values. If we set the derivative of $Re[\varepsilon(E)]$ (Equation S9) with respect to the variable $Eo - E$ equal to zero, it follows that the extreme values of $Re[\varepsilon(E)]$, $Re[\varepsilon(E)]max = 1+ Im[\varepsilon(E)]max$, and $Re[\varepsilon(E)]min = 1- Im[\varepsilon(E)]max$ occur at $E = Eo -\Gamma$ and $E = Eo +\Gamma$, respectively. In addition, $Im[\varepsilon(E)]$ tends towards 0 away from its peak maximum energy. We further obtained the magnitude of the amplitude as shown in Figure 3D. Like the LSPR peaks linewidths, the amplitudes show maximum values at resonance and a significant damping effect (Figures S5D, S6D and S7D for full details). It is notable via the oscillators strength ($Im[\varepsilon(E)]$ intensities) that the observed IB transitions are weak. Indeed, the stronger the IB transition, the higher $Re[\varepsilon(\omega)]>>1$ and the smaller $Im[\varepsilon(E)]$[Toudert, 2017 #120;Toudert, 2017 #138].

Figure 4A shows that AuBPs exhibit high IB transition oscillator strength in oil RI as illustrated by the amplitude in Figure 3D, followed by water, and then air RI. As a result, Figure 4B shows that the real part ($Re[\varepsilon(\omega)]$) of AuBP IB transitions becomes strongly negative ($Re[\varepsilon(E)]<0$ and small $Im[\varepsilon(E)]$) for oil (green hatched part) followed by water (blue hatched part) and then air (blue hatched part) RI at photon energies higher than the resonance peak maxima (condition to achieve

plasmonic resonance) as shown in Figures 4A-4B. At photon energies lower than the resonance peak maxima, they take high positive values ($Re[\varepsilon(\omega)]>0$) (Figure 4B) in the same order. The conditions for achieving Mie resonances, $Re[\varepsilon(\omega)]>>1$ and small $Im[\varepsilon(E)]$ are not fulfilled due to the weak value of the oscillator strength and because we are under the subwavelength scattering of our AuBPs. This suggests that only the IB transitions originating from plasmons contribute to the resonance in single AuBPs with the dominated intra-band transitions calculated by the use of Johnson and Christy data, as shown in Figures 4C-4D. The extent of their LSPR quality factors is shown in Figure 4C and magnified in Figure 4D for better illustration in the three RI media. These results reveal that a small increase in the RI of the surrounding medium effectively increases the quality factor of the LSPR due to IB transitions. Thus, IB transitions of oil RI yields a higher quality factor followed by water RI. The plasmonic quality factor gives a qualitative picture of the capability of nanostructures of a material to support a well-defined LSPR at a chosen photon energy. The higher the quality factor, the higher the probability of obtaining a spectrally sharp resonance with a strong optical near field that can exist at the chosen photon energy. It is noteworthy that neglecting IB transitions can work for an air RI medium, whereas in a high RI medium its contribution can be underestimated.

Although the observed IB transitions are weak, as they have Lorentzian shape like LSPR peaks and first derivatives, they helped us by analytically treating the imaginary and real parts like LSPR scattering and its first derivative as they are used above in Figures 2A-2C to investigate IF sensitivity and damping. Figures 5A-5C show the changes of the Kramers-Kronig consistent Lorentz based complex dielectric functions (Figures S5A-S5B, S6A- S6B and S7A- S7B for full details) around single gold bipyramids in different local RI media near their resonance energies. The first line represents the imaginary part and the second line represents the real part. As for the LSPR spectra and their first and second derivative components, the columns are differentiated by three colors with each corresponding to a different local RI medium, red for air, blue for water, and green for oil. As mentioned previously, the LSPR peak maxima are assimilated to the imaginary part of the complex dielectric function in the three local refractive index media represented by capital B. The local

maxima and minima of the real part of the complex dielectric function flanking the LSPR peak maxima are represented by A and C, respectively.

This result is consistent with those we obtained for single gold LSPR scattering located above. Moreover, a quantitative assessment of the shifts based on discrete dipole approximation calculations performed on the oscillatory dependence of the peak shift on wavelength tracks with the wavelength dependence of the real part of the refractive index, determined by the Kramers-Kronig transformation of the molecular absorption spectrum, showed that the Kramers-Kronig index needed to be scaled to better match experimental data[56]. However, the present results highlight the observation for changes of the real part of the complex dielectric functions in the surroundings of single nanoparticles and are in good agreement with another report on the scaling of Kramers-Kronig transformations[56].

Similar to the single gold LSPR scattering, in the regime relevant to sensing properties, the peaks energies are also with good approximation linear functions of local RI media, as shown in Figure 5D. The exhibited sensitivity is slightly higher than that of single gold LSPR scattering. Indeed, the linear function fitting yielded slope values equal to 0.54 eV·RIU^{-1} (R^2 = 0.9876) for peak A, 0.64 eV·RIU^{-1} (R^2 = 0.9870) for peak B and 0.74 eV·RIU^{-1} (R^2 = 0.9871) for peak C. As seen in Figure 5E, the peak energies C exhibited the highest sensitivity compared to both, A and the resonance peaks B with a local RI sensitivity improvement of 15.63% with respect to the resonance peaks. Although for the single gold LSPR scattering the peaks A and C showed almost the same values of improvement, for changes of the complex dielectric functions, the peak maximum B shows better sensitivity than A with an improvement of 18.36%. This result could be justified by the changes of the phases against photon energy. The high slopes of the two tangent lines on A and C in Figure 5F show how the phases readily change (see Figures S5C, S6C and S7C for full details) for a slight change in the range of photon energies where IB transition contributions decrease.

Although in one hand we have demonstrated the tracking of curve changes and its IF C by the use of single particle scattering spectra, and on the other hand that monitoring the dielectric changes and its local minima peaks C enhances

the local RI sensitivity, to better understand the performance of the phase stability at peaks A, B, and C relative to the performance of sensitivity, we analyzed the effect of the signal-to-noise ratio. In a sensing experiment, both the sensitivity and the noise of the sensor determine the performance of the method[57]. For full details, the results of the analysis are shown in Tables S1~S4 and are summarized in Figure 6 with the IB transitions.As seen for the two methods, the curvature changes and the dielectric change peaks A, B, and C did not significantly propagate the noise. Tracking IF points as well as the changing of the dielectric function in the vicinity of single gold bipyramids enhanced the sensitivity. These results show that not only the low noise level and high quality of the original scattering spectra, but also the improvement in signal-to-noise ratio of sensing by single AuBPs in the three local refractive indexes, are represented by the improvement in sensitivity.

Conclusion

In summary, we have demonstrated for a AuBP embedded in various local refractive indexes the importance of tracking the curvature shapes through inflection points near the resonance energy unlike LSPR peaks. In addition, we also evaluated the IB transition contributions in the frequency range dominated by intra-band transitions. The inflection point frequencies exhibited enhanced sensitivity in high phase steady state range compared to monitoring resonance shifts. A small increase in the local RI significantly increases the IB transition contributions to the LSPR as well as related optical property measurements. These findings support the idea that tracking curvatures of an optical signal can be used effectively for longitudinal sharpened peak energy LSPR RI sensing as well as for damping in the local RI environment of single AuBPs and other anisotropic nanoparticles with a single resonant mode. Furthermore, the effect on IB transition contributions should be taken into account when working with high refractive index media.

References

1. Fong, K. E.; Yung, L.-Y. L., Localized surface plasmon resonance: a unique property of plasmonic nanoparticles for nucleic acid detection. *Nanoscale* **2013,***5* (24), 12043-12071.

2. Doria, G.; Conde, J.; Veigas, B.; Giestas, L.; Almeida, C.; Assunção, M.; Rosa, J.; Baptista, P. V., Noble Metal Nanoparticles for Biosensing Applications. *Sensors (Basel, Switzerland)* **2012,***12* (2), 1657-1687.
3. Jana, J.; Ganguly, M.; Pal, T., Enlightening surface plasmon resonance effect of metal nanoparticles for practical spectroscopic application. *RSC Advances* **2016,***6* (89), 86174-86211.
4. Willets, K. A.; Van Duyne, R. P., Localized surface plasmon resonance spectroscopy and sensing. *Annual review of physical chemistry* **2007,***58*, 267-97.
5. Zhang, X.-F.; Liu, Z.-G.; Shen, W.; Gurunathan, S., Silver Nanoparticles: Synthesis, Characterization, Properties, Applications, and Therapeutic Approaches. *International Journal of Molecular Sciences* **2016,***17* (9), 1534.
6. (a) Li, M.-C.; Chang, Y.-F.; Wang, H.-Y.; Lin, Y.-X.; Kuo, C.-C.; Annie Ho, J.-a.; Lee, C.-C.; Su, L.-C., An innovative application of time-domain spectroscopy on localized surface plasmon resonance sensing. *Scientific Reports* **2017,***7*, 44555; (b) Jeppesen, C.; Lindstedt, D. N.; Laurberg, A. V.; Kristensen, A.; Mortensen, N. A. In *Nanometrology using localized surface plasmon resonance spectroscopy*, 2013 Conference on Lasers & Electro-Optics Europe & International Quantum Electronics Conference CLEO EUROPE/IQEC, 12-16 May 2013; 2013; pp 1-1.
7. Gabudean, A. M.; Biro, D.; Astilean, S., Localized surface plasmon resonance (LSPR) and surface-enhanced Raman scattering (SERS) studies of 4-aminothiophenol adsorption on gold nanorods. *Journal of Molecular Structure* **2011,***993* (1), 420-424.
8. Chamanzar, M.; Adibi, A. In *On-chip localized surface Plasmon resonance (LSPR) sensing*, IEEE Photonic Society 24th Annual Meeting, 9-13 Oct. 2011; 2011; pp 153-154.
9. Bauch, M.; Toma, K.; Toma, M.; Zhang, Q.; Dostalek, J., Plasmon-Enhanced Fluorescence Biosensors: a Review. *Plasmonics* **2014,***9* (4), 781-799.
10. Yonzon, C. R.; Zhang, X.; Duyne, R. P. V. In *Localized surface plasmon resonance immunoassay and verification using surface-enhanced Raman spectroscopy*, Optical Science and Technology, SPIE's 48th Annual Meeting, SPIE: 2003; p 8.

11. Unser, S.; Bruzas, I.; He, J.; Sagle, L., Localized Surface Plasmon Resonance Biosensing: Current Challenges and Approaches. *Sensors (Basel, Switzerland)* **2015,***15* (7), 15684-15716.
12. Yokota, H.; Taniguchi, T.; Watanabe, T.; Kim, D., Control of localized surface plasmon resonance energy in monolayer structures of gold and silver nanoparticles. *Physical Chemistry Chemical Physics* **2015,***17* (40), 27077-27081.
13. Gu, X.; Qiu, T.; Zhang, W.; Chu, P. K., Light-emitting diodes enhanced by localized surface plasmon resonance. *Nanoscale Research Letters* **2011,***6* (1), 199-199.
14. Li, J.; Cushing, S. K.; Zheng, P.; Meng, F.; Chu, D.; Wu, N., Plasmon-induced photonic and energy-transfer enhancement of solar water splitting by a hematite nanorod array. *Nature Communications* **2013,***4*, 2651.
15. Yu, M.; Yang, C.; Li, X.-M.; Lei, T.-Y.; Sun, H.-X.; Dai, L.-P.; Gu, Y.; Ning, X.; Zhou, T.; Wang, C.; Zeng, H.-B.; Xiong, J., Universal liquid-phase laser fabrication of various nano-metals encapsulated by ultrathin carbon shells for deep-UV plasmonics. *Nanoscale* **2017,***9* (25), 8716-8722.
16. Lee, Y.; Kim, S.-J.; Park, H.; Lee, B., Metamaterials and Metasurfaces for Sensor Applications. *Sensors (Basel, Switzerland)* **2017,***17* (8), 1726.
17. Arvizo, R.; Bhattacharya, R.; Mukherjee, P., Gold nanoparticles: Opportunities and Challenges in Nanomedicine. *Expert opinion on drug delivery* **2010,***7* (6), 753-763.
18. Jazayeri, M. H.; Amani, H.; Pourfatollah, A. A.; Pazoki-Toroudi, H.; Sedighimoghaddam, B., Various methods of gold nanoparticles (GNPs) conjugation to antibodies. *Sensing and Bio-Sensing Research* **2016,***9*, 17-22.
19. Lee, D.-E.; Koo, H.; Sun, I.-C.; Ryu, J. H.; Kim, K.; Kwon, I. C., Multifunctional nanoparticles for multimodal imaging and theragnosis. *Chemical Society Reviews* **2012,***41* (7), 2656-2672.
20. Olson, J.; Dominguez-Medina, S.; Hoggard, A.; Wang, L.-Y.; Chang, W.-S.; Link, S., Optical Characterization of Single Plasmonic Nanoparticles. *Chemical Society reviews* **2015,***44* (1), 40-57.
21. Mody, V. V.; Siwale, R.; Singh, A.; Mody, H. R., Introduction to metallic nanoparticles. *Journal of Pharmacy and Bioallied Sciences* **2010,***2* (4), 282-289.

22. de Melo, P. B.; Nunes, A. M.; Omena, L.; Nascimento, S. M. S. d.; da Silva, M. G. A.; Meneghetti, M. R.; de Oliveira, I. N., Thermo-optical properties and nonlinear optical response of smectic liquid crystals containing gold nanoparticles. *Physical Review E* **2015,***92* (4), 042504.
23. Sperling, R. A.; Parak, W. J., Surface modification, functionalization and bioconjugation of colloidal inorganic nanoparticles. *Philosophical Transactions of the Royal Society A: Mathematical, Physical and Engineering Sciences* **2010,***368* (1915), 1333.
24. Chen, Y.; Xianyu, Y.; Jiang, X., Surface Modification of Gold Nanoparticles with Small Molecules for Biochemical Analysis. *Accounts of chemical research* **2017,***50* (2), 310-319.
25. Curry, T.; Kopelman, R.; Shilo, M.; Popovtzer, R., Multifunctional theranostic gold nanoparticles for targeted CT imaging and photothermal therapy. *Contrast Media & Molecular Imaging* **2014,***9* (1), 53-61.
26. Jans, H.; Huo, Q., Gold nanoparticle-enabled biological and chemical detection and analysis. *Chemical Society Reviews* **2012,***41* (7), 2849-2866.
27. Bharadwaj, R.; Tripathi, R.; Prabhakar, A.; Mukherji, S., *S-shaped SU-8 optical waveguide immobilized with gold nanoparticles for trace detection of explosives*. 2013; Vol. 8924, p 892424.
28. Bok, H. M.; Shuford, K. L.; Kim, S.; Kim, S. K.; Park, S., Multiple surface plasmon modes for gold/silver alloy nanorods. *Langmuir : the ACS journal of surfaces and colloids* **2009,***25* (9), 5266-70.
29. Schneider, T.; Jahr, N.; Jatschka, J.; Csaki, A.; Stranik, O.; Fritzsche, W., Localized surface plasmon resonance (LSPR) study of DNA hybridization at single nanoparticle transducers. *Journal of Nanoparticle Research* **2013,***15* (4), 1531.
30. Ringe, E.; Sharma, B.; Henry, A.-I.; Marks, L. D.; Van Duyne, R. P., Single nanoparticle plasmonics. *Physical Chemistry Chemical Physics* **2013,***15* (12), 4110-4129.
31. Kleinman, S. L.; Bingham, J. M.; Henry, A.-I.; Wustholz, K. L.; Duyne, R. P. V. In *Structural and optical characterization of single nanoparticles and single molecule SERS*, SPIE NanoScience + Engineering, SPIE: 2010; p 10.

32. Li, Q.; Zhuo, X.; Li, S.; Ruan, Q.; Xu, Q.-H.; Wang, J., Production of Monodisperse Gold Nanobipyramids with Number Percentages Approaching 100% and Evaluation of Their Plasmonic Properties. *Advanced Optical Materials* **2015,***3* (6), 801-812.
33. Derkachova, A.; Kolwas, K.; Demchenko, I., Dielectric Function for Gold in Plasmonics Applications: Size Dependence of Plasmon Resonance Frequencies and Damping Rates for Nanospheres. *Plasmonics (Norwell, Mass.)* **2016,***11*, 941-951.
34. Nehl, C. L.; Hafner, J. H., Shape-dependent plasmon resonances of gold nanoparticles. *Journal of Materials Chemistry* **2008,***18* (21), 2415-2419.
35. Ringe, E.; M. McMahon, J.; Sohn, K.; Cobley, C.; Xia, Y.; Huang, J.; C. Schatz, G.; D. Marks, L.; P. Van Duyne, R., *Unraveling the Effects of Size, Composition, and Substrate on the Localized Surface Plasmon Resonance Frequencies of Gold and Silver Nanocubes: A Systematic SingleParticle Approach*. 2010; Vol. 114, p 12511-12516.
36. Wang, Y.; Tang, L., Chemisorption Assembly of Au Nanorods on Mercaptosilanized Glass Substrate for Label-free Nanoplasmon Biochip. *Analytica chimica acta* **2013,***796*, 10.1016/j.aca.2013.08.024.
37. Soares, L.; Csaki, A.; Jatschka, J.; Fritzsche, W.; Flores, O.; Franco, R.; Pereira, E., Localized surface plasmon resonance (LSPR) biosensing using gold nanotriangles: detection of DNA hybridization events at room temperature. *Analyst* **2014,***139* (19), 4964-4973.
38. Nusz, G. J.; Curry, A. C.; Marinakos, S. M.; Wax, A.; Chilkoti, A., Rational Selection of Gold Nanorod Geometry for Label-Free Plasmonic Biosensors. *ACS nano* **2009,***3* (4), 795-806.
39. Hu, M.; Novo, C.; Funston, A.; Wang, H.; Staleva, H.; Zou, S.; Mulvaney, P.; Xia, Y.; Hartland, G. V., Dark-field microscopy studies of single metal nanoparticles: understanding the factors that influence the linewidth of the localized surface plasmon resonance. *Journal of materials chemistry* **2008,***18* (17), 1949-1960.
40. Yang, S.; Wu, T.; Zhao, X.; Li, X.; Tan, W., The Optical Property of Core-Shell Nanosensors and Detection of Atrazine Based on Localized Surface Plasmon

Resonance (LSPR) Sensing. *Sensors (Basel, Switzerland)* **2014,***14* (7), 13273-13284.

41. Otte, M. A.; Sepulveda, B., Figures of Merit for Refractometric LSPR Biosensing. In *Nanoplasmonic Sensors*, Dmitriev, A., Ed. Springer New York: New York, NY, 2012; pp 317-331.
42. Chen, P.; Liedberg, B., Curvature of the localized surface plasmon resonance peak. *Analytical chemistry* **2014,***86* (15), 7399-405.
43. Derkachova, A.; Kolwas, K.; Demchenko, I., Dielectric Function for Gold in Plasmonics Applications: Size Dependence of Plasmon Resonance Frequencies and Damping Rates for Nanospheres. *Plasmonics* **2016,***11* (3), 941-951.
44. Alabastri, A.; Tuccio, S.; Giugni, A.; Toma, A.; Liberale, C.; Das, G.; Angelis, F.; Fabrizio, E. D.; Zaccaria, R. P., Molding of Plasmonic Resonances in Metallic Nanostructures: Dependence of the Non-Linear Electric Permittivity on System Size and Temperature. *Materials (Basel, Switzerland)* **2013,***6* (11), 4879-4910.
45. Amendola, V.; Pilot, R.; Frasconi, M.; Marago, O. M.; Iati, M. A., Surface plasmon resonance in gold nanoparticles: a review. *Journal of physics. Condensed matter : an Institute of Physics journal* **2017,***29* (20), 203002.
46. Tavakol, P., Optical absorption of nanoparticles described by an electronic local interband transition. *Journal of Optics* **2013,***15* (2), 025001.
47. Foerster, B.; Joplin, A.; Kaefer, K.; Celiksoy, S.; Link, S.; Sönnichsen, C., Chemical Interface Damping Depends on Electrons Reaching the Surface. *ACS nano* **2017,***11* (3), 2886-2893.
48. Chen, P.; Tran, N. T.; Wen, X.; Xiong, Q.; Liedberg, B., Inflection Point of the Localized Surface Plasmon Resonance Peak: A General Method to Improve the Sensitivity. *ACS sensors* **2017,***2* (2), 235-242.
49. Juve, V.; Cardinal, M. F.; Lombardi, A.; Crut, A.; Maioli, P.; Perez-Juste, J.; Liz-Marzan, L. M.; Del Fatti, N.; Vallee, F., Size-dependent surface plasmon resonance broadening in nonspherical nanoparticles: single gold nanorods. *Nano letters* **2013,***13* (5), 2234-40.
50. Lee, J.-H.; Gibson, K. J.; Chen, G.; Weizmann, Y., Bipyramid-templated synthesis of monodisperse anisotropic gold nanocrystals. *Nature Communications* **2015,***6*, 7571.

51. Pakizeh, T., Optical Absorption of Plasmonic Nanoparticles in Presence of a Local Interband Transition. *The Journal of Physical Chemistry C* **2011,***115* (44), 21826-21831.
52. Lovell, R., Application of Kramers-Kronig relations to the interpretation of dielectric data. *Journal of Physics C: Solid State Physics* **1974,***7* (23), 4378;
53. McFarland, A. D.; Van Duyne, R. P., Single Silver Nanoparticles as Real-Time Optical Sensors with Zeptomole Sensitivity. *Nano letters* **2003,***3* (8), 1057-1062.
54. Ha, J. W., Chemical interface damping of single gold nanorods with low sensitivity to the medium dielectric constant. *Chemical Physics Letters* **2017,***676*, 65-69.
55. Bakhti, S.; Destouches, N.; Tishchenko, A. V., Modeling and Interpretation of Hybridization in Coupled Plasmonic Systems. In *Reviews in Plasmonics 2015*, Geddes, C. D., Ed. Springer International Publishing: Cham, 2016; pp 19-49.
56. Haes, A. J.; Zou, S.; Zhao, J.; Schatz, G. C.; Van Duyne, R. P., Localized surface plasmon resonance spectroscopy near molecular resonances. *J Am Chem Soc* **2006,***128* (33), 10905-14.
57. He, Y. J., High-Performance LSPR Fiber Sensor Based on Nanometal Rings. *IEEE Photonics Journal* **2014,***6* (2), 1-11.

Figures and Captions

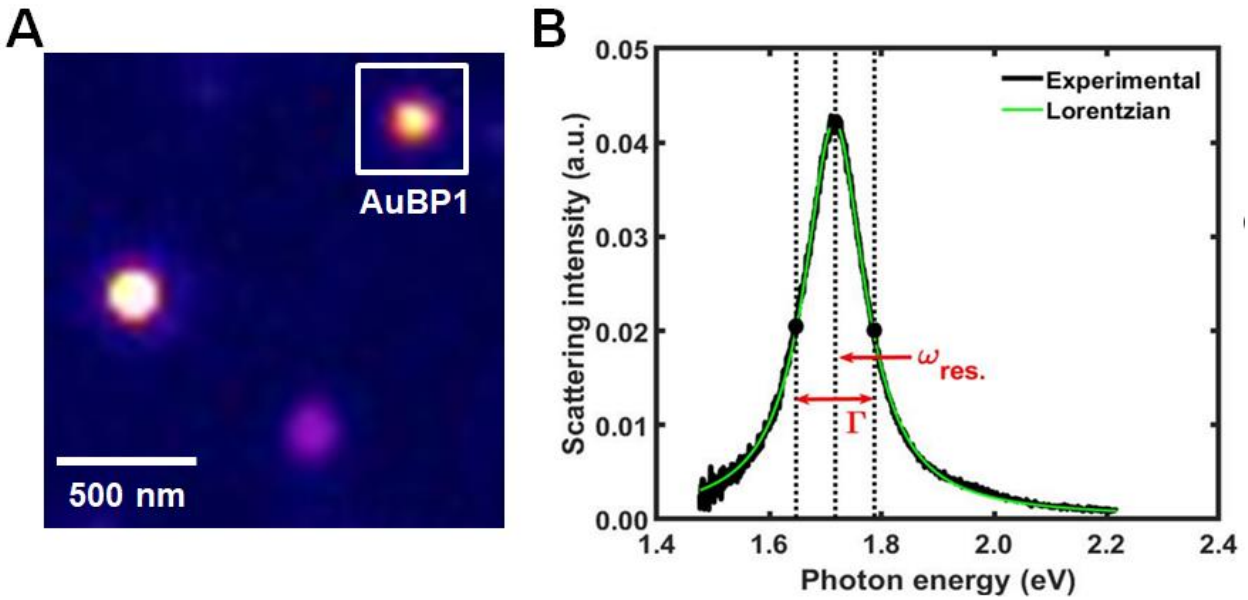

Figure1. *Dark-field microscopy and spectroscopy of single gold bipyramids. (A) Dark-field image of single AuBPs excited by white light illumination. (B) Scattering spectrum of a AuBP1 in water refractive index. The line shape (black-curve) is well fitted by the Lorentzian function (green-curve). The extraction of the resonance energy ($\omega_{res.}$)as well as the full width at half maximum (FWHM) isillustrated.*

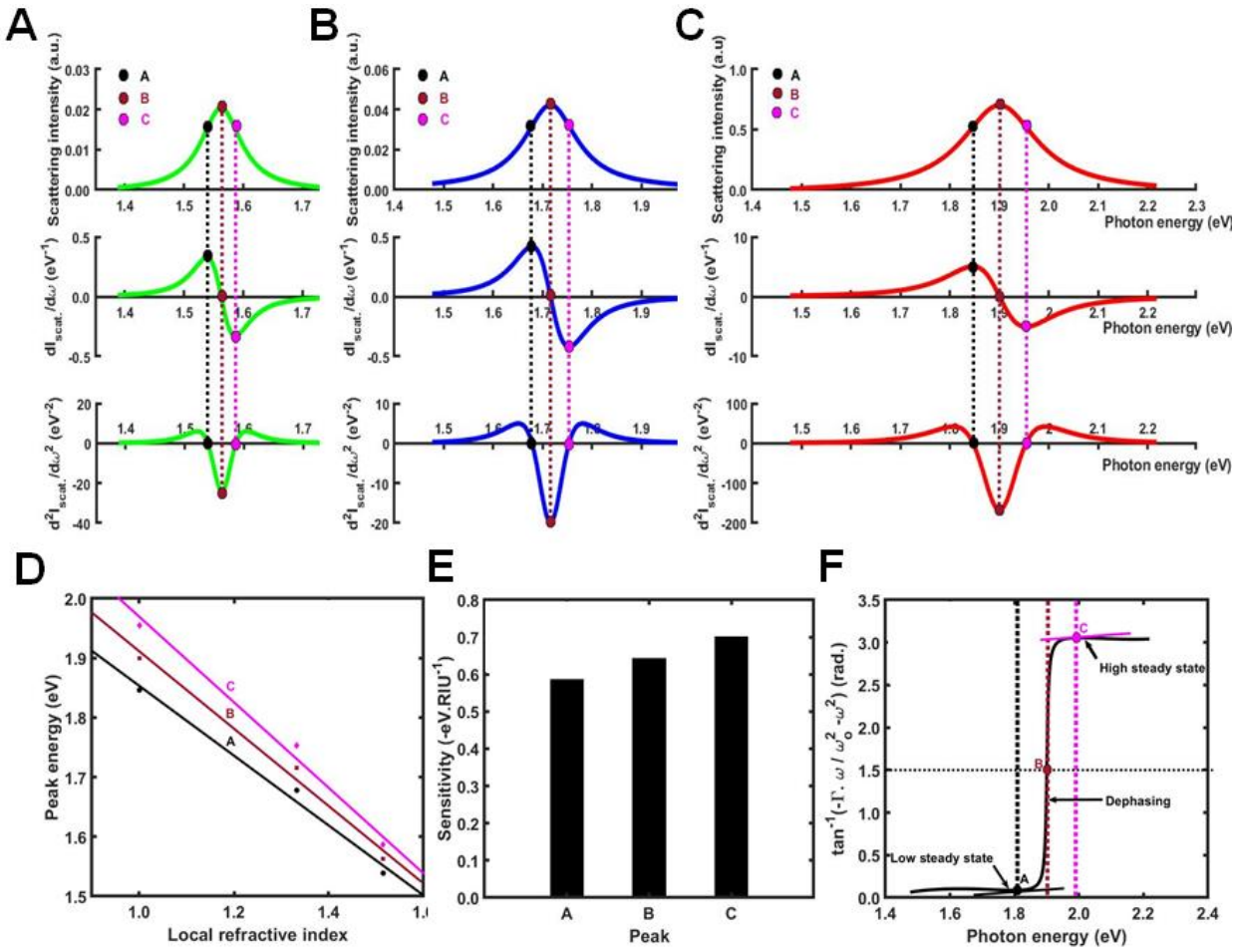

Figure 2. *Inflection point method for single particle LSPR scattering sensing and damping in the three local refractive indexes, namely, air (red), water (blue), and oil (green). (A), (B), and (C) LSPR scattering efficiencies (first row), LSPR scattering efficiencies first order derivatives (second row), and LSPR scattering efficiencies second order derivatives (third row). (D) LSPR scattering efficiencies, LSPR scattering efficiencies first order derivatives and LSPR scattering efficiencies second order derivative energy peaks A, B and C linearly related to local RI media in regimes relevant to sensing. (E) Sensitivity of local RI media on Peak shifts A, B and C. (F) Phase changes around the resonance/LSPR energy illustrated for a single AuBP embedded in local air RI medium and illustration of the two low slope phase*

tangents on peaks A and C located near the high (pink) and low (black) phase steady state.

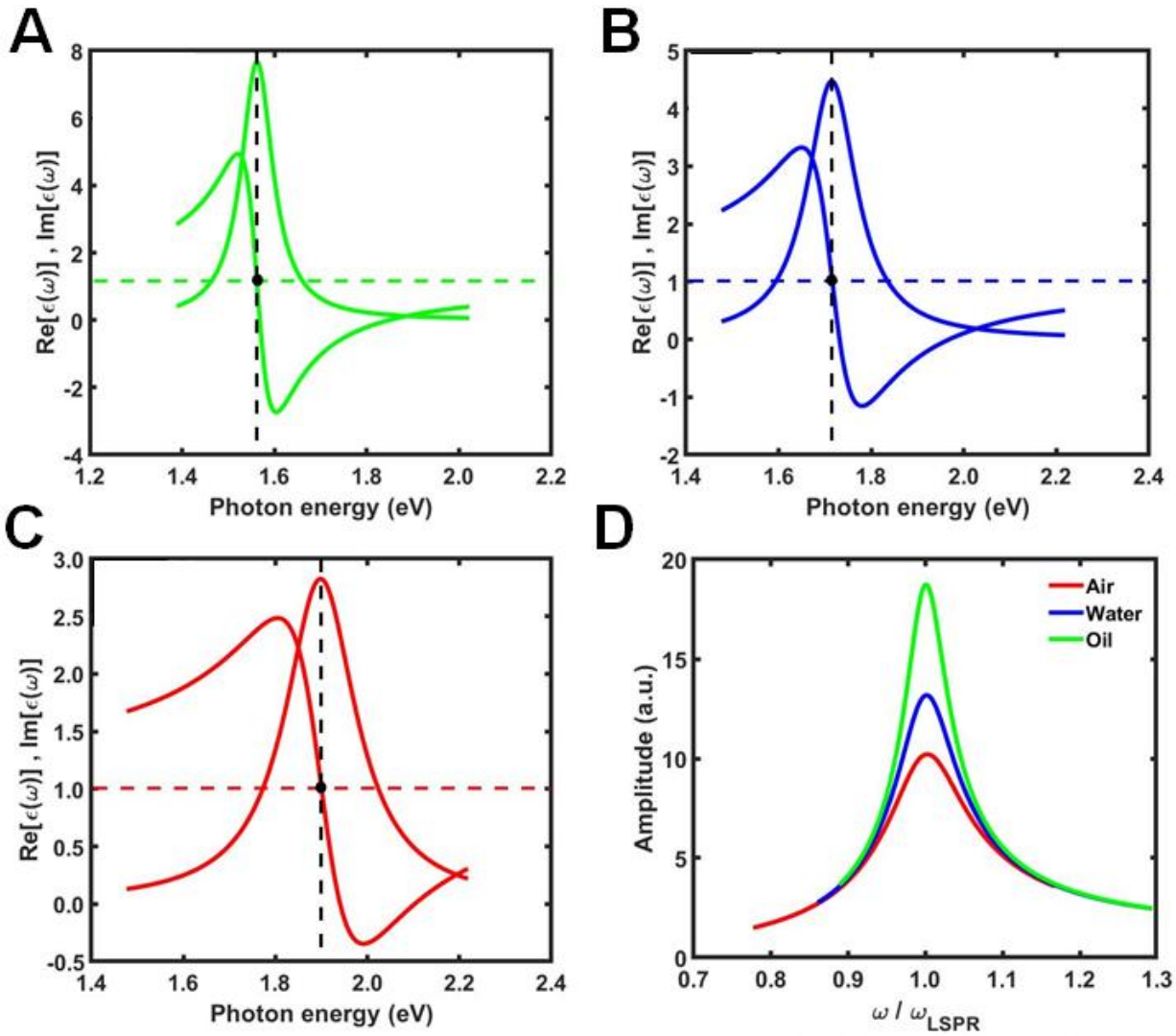

Figure 3. *Dielectric function changes around AuNPs embedded in air (red) (A), water (blue) (B) and oil (green) (C) against the energy near their resonance/LSPR energy, derived from the dipole approximation of the Lorentz model based on Kramers-Kronig transformations (D) Resonance amplitude against normalized frequency. The largest damping (oil) giving the sharpest resonance curve.*

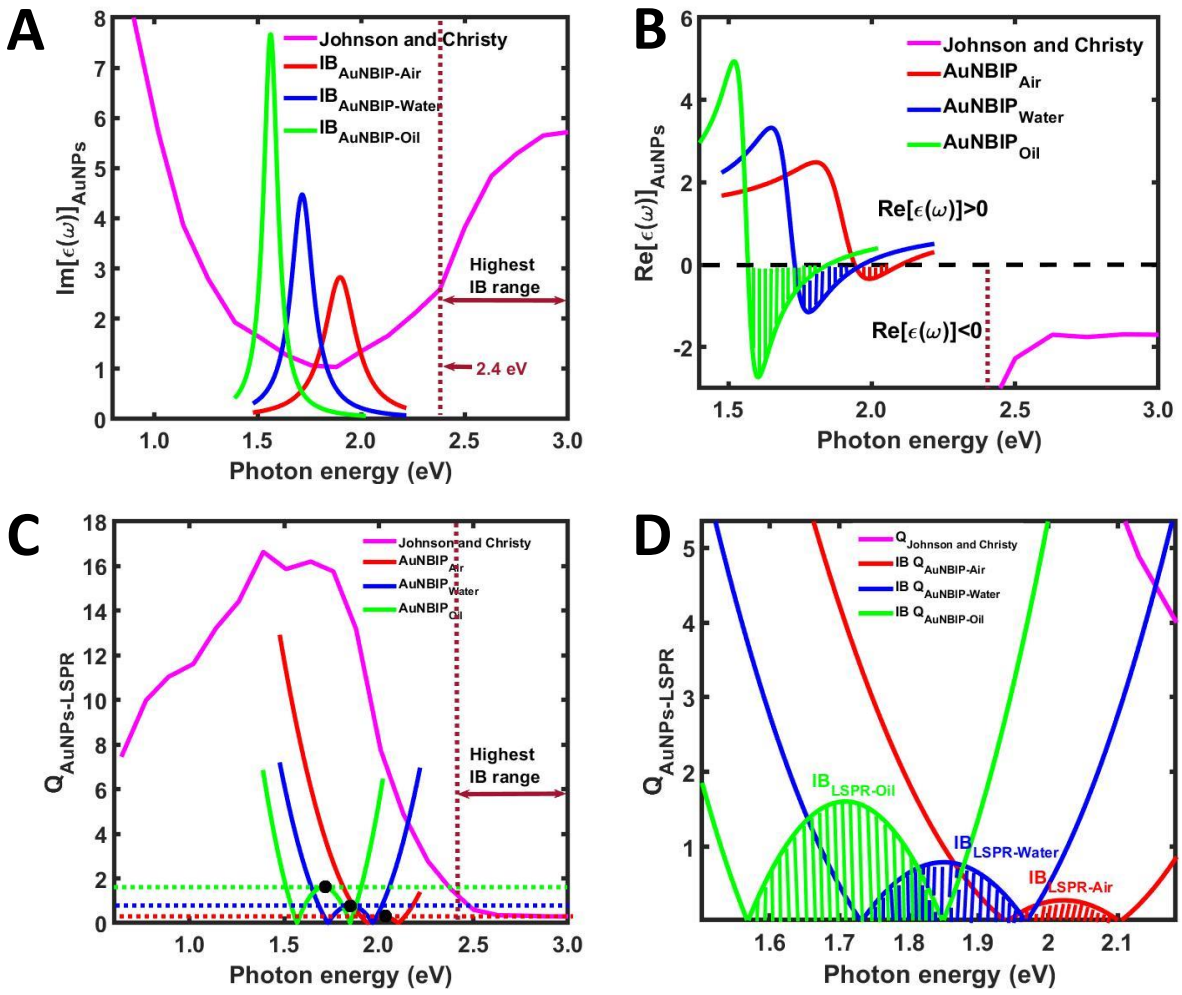

Figure 4. *IB transition contributions affecting the corresponding plasmon excitations in the frequency range dominated by intra-band electronic transitions. (A) IB transitions with various oscillation strengths derived in the frequency range where they are usually neglected as illustrated by the imaginary part of the dielectric calculated by Johnson and Christy data. The colors are associated with RI media. (B) Negative real part due to IB that interferes with intra-band electronic transitions. (C) LSPR quality factor due to the IB contributions and magnified in (D).*

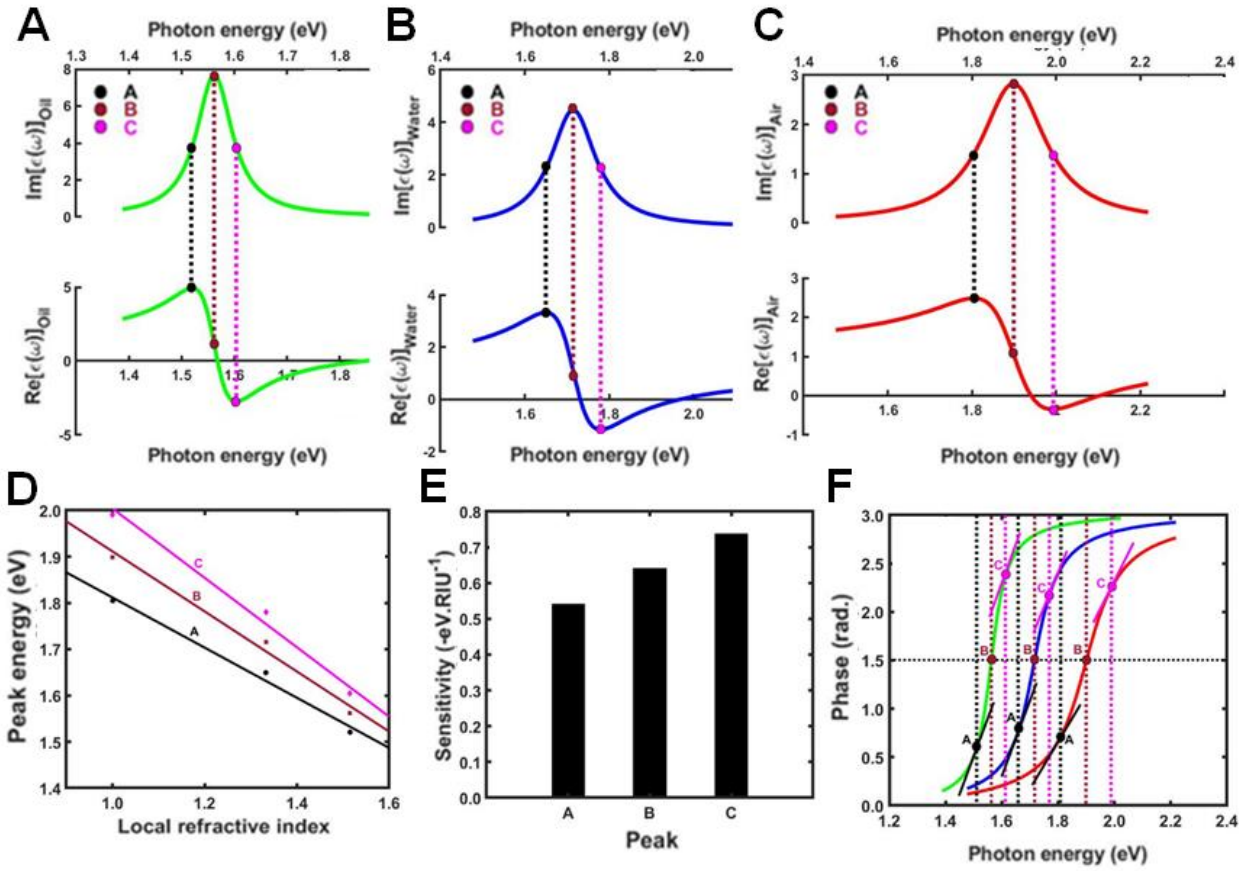

Figure 5. Relationship between the imaginary parts and the real parts of Lorentz's dielectric function with respect to the LSPR and IFs energies. (A), (B) and (C) Imaginary parts (first row), the real parts (second row). (D) Resonance energies, Im[ε(ω)]max peak energies and Re[ε(ω)]max/min peak energies A, B and C linearly related to local RI media in regimes relevant to sensing. (E) Sensitivity of local RI media on Peak shifts A, B and C. (F) Phase changes around the resonance/LSPR energy.

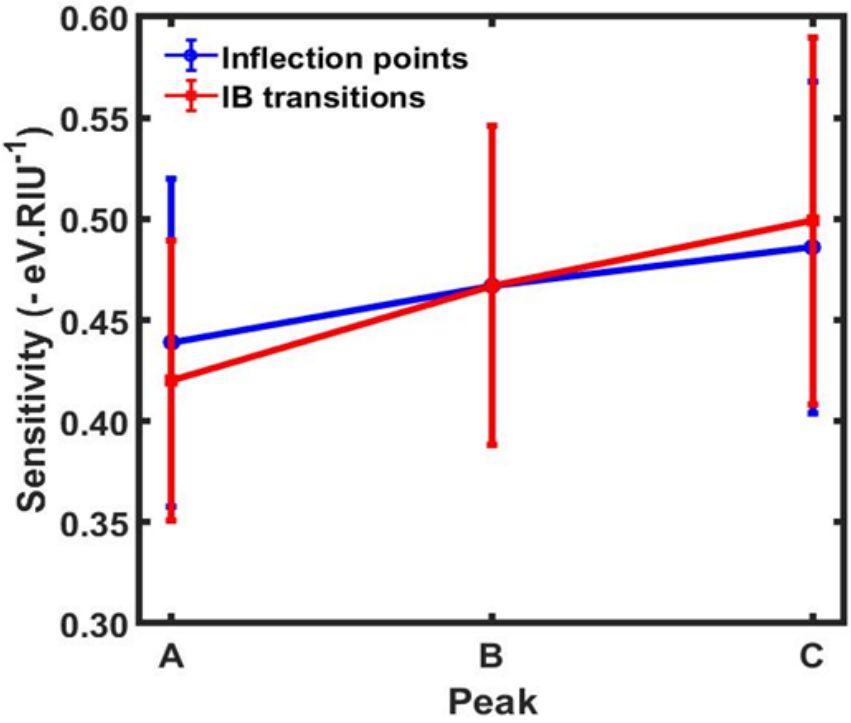

Figure 6. *Performances of LSPR shifts, LSPR inflection points, and IB transition contributions. Analysis of sensitivity on the curvature and dielectric function changes for the three peaks A, B, and C for LSPR inflection points and dielectric function changes with regard to noise effects.*

Supplementary Materials

Electrodynamic for Gold Bipyramids and LSPR Inflection Points

For nanoparticles the optical cross sections as a function of energy are dominated by the localized surface plasmon resonance[1]. At the resonance energy (or wavelength), the peak position and linewidth are determined by the size and shape of nanoparticle as well as the dielectric surrounding environment. By solving Maxwell's equations using Mie theory and considering only the lowest dipolar mode (dipolar approximation) the scattering cross section solution can varies for different shapes of nanoparticles characterized by a frequency-dependent complex dielectric function $\varepsilon_{1(\omega)} + \varepsilon_{2(\omega)}$ embedded in a medium of dielectric $\varepsilon_m = n_m^2$.[1-2] For an ellipsoid

(such as bipyramids) along one of its main axis, the extinction cross section in the dipolar approximation is well described by the analytical expression given by the equation (1)[3]:

$$\sigma_{ext}(\lambda) = \frac{2\pi V n_m^{\,3}}{\lambda\beta^2} \frac{\varepsilon_2(\lambda)}{\left|\varepsilon(\lambda) + \frac{1-\beta}{\beta} n_m^{\,2}\right|^2} \quad (1)$$

where β is a shape-dependent factor (only depend on the aspect ratio for nano-spheroid). For a weakly dispersed $\varepsilon_{2(\lambda)}$ around the LSPR peak maximum (λ_{res}) (e.g., away from the inter-band absorption), the resonance condition is well approximated by $\varepsilon_1(\lambda_{res.}) \approx (\beta-1) n_m^{\,2} / \beta$. The LSPR width can then be estimated developing equation (1) around the LSPR frequency[3-4] ω_{res} to obtain equation (2):

$$\sigma_{ext}(\lambda) = \frac{\omega V n_m^{\,3}}{2c\beta^2 \left(\partial\varepsilon_1 / \partial\omega\right)_{\omega_{res.}}} \frac{\Gamma}{\left(\omega - \omega_{res.}\right)^2 + \left(\Gamma/2\right)^2} \quad (2)$$

With the angular frequency $\omega=(2\pi c/\lambda)$. The LSPR thus exhibits a quasi-Lorentzian profile[1, 3] with a full width at half maximum (FWHM) Γ that took the same form as in gold bipyramidsfrom our results and given by the Lorentzian fitting curves:

$$I_{Scat.} = I_0 + \left(\frac{2A}{\pi}\right) \frac{\Gamma}{4\left(\omega - \omega_{res.}\right)^2 + \Gamma^2} \quad (3)$$

Where I_o and A are offset and area under the peak, respectively. In a nano-sphere under the same approximations[4]:

$$\Gamma = 2\varepsilon_2(\omega_{res.}) \Big/ \left(\partial\varepsilon_1 / \partial\omega\right)_{\omega_{res.}} \quad (4)$$

The LSPR scattering spectra were fitted with the use of a Lorentzian function depicted by equation (3) to determine the LSPR linewidth Γ and the resonance

frequency ω_{res}. First and second order derivative of the LSPR scattering spectra were performed by the use of equations (5) and (6), respectively.

$$\frac{dI_{Scat.}}{d\omega} = -\left(\frac{16A}{\pi}\right)\frac{\left(\omega-\omega_{res.}\right)\omega}{\left[4\left(\omega-\omega_{res.}\right)^2+\Gamma^2\right]^2} \quad (5)$$

$$\frac{d^2I_{Scat.}}{d\omega^2} = -\left(\frac{16A}{\pi}\right)\frac{\left[\Gamma^2-12\left(\omega-\omega_{res.}\right)^2\right]\omega}{\left[4\left(\omega-\omega_{res.}\right)^2+\Gamma^2\right]^3} \quad (6)$$

For every first and second derivation, the local maximum/maximum and inflection points were extracted for peak energies analysis. The FWHM obtained between the two inflection points were in good agreement with that of equation (3).

Changes of theComplex Dielectric Functions

The changes in the complex dielectric functions in the vicinity of single gold bipyramids embedded local RI media used in this work is introduced by considering Kramers-Kronig consistent Lorentz transformations[5]. In the light absorption and scattering by small particles experiments, the real and imaginary parts of optical properties that are frequency-dependent complex functions of the driving electric field such as polarizability[6], dielectric[7] and refractive index[8] are related. For instance, in the positives frequencies ranges, the changes of real and imaginary parts of complex polarizability functions can be break down in equation (7) and (8) expressed by dispersion relations[9], and are called Kramers-Kronig transformations[5].

$$\chi_r(\omega) = \frac{2}{\pi}P\int_0^\infty \frac{\Omega\chi_i(\omega)}{\Omega^2-\omega^2}d\Omega \quad (7)$$

$$\chi_i(\omega) = -\frac{2\omega}{\pi}P\int_0^\infty \frac{\Omega\chi_r(\omega)}{\Omega^2-\omega^2}d\Omega \quad (8)$$

Where χ_i, χ_r, ω, Ω and P indicate the frequency-dependent imaginary part, the frequency-dependent real part, the angular frequency ($2\pi c/\lambda$), a parameter

related to the change in the absorption coefficient[8] and the principal value of the integral, respectively. The frequency-dependent real and imaginary parts are connected by integrations. This analytic property imposes a constraint on physically realizable susceptibility/polarizabilities or others optical responses, since the optical constants must satisfy Kramers-Kronig relation[10] (or dispersion relations) to be physical[11].In this relation, if the frequency-dependent real part is known over a sufficiently large range of angular frequencies ω, the frequency-dependent imaginary part can be obtained by integration, and vice versa, that is, one is the derivative of another[12].The change of analytic relative frequency-dependent complex dielectric function is then obtained by $\varepsilon_r = 1 + \chi$ and integrals in equations (7) and (8) relate area under the frequency-dependent imaginary part of the complex dielectric or susceptibility/polarizability functions to shape of frequency-dependent real part of the complex dielectric and vice-versa[13]. From the same theory (S1) it was inferred from the Lorentzian form of both, scattering cross section and absorption cross section that the real part of the dielectric function determines the plasmon resonance position whereas the imaginary part governs the linewidth[1].Therefore, using this dipole approximation equation, we derived both the real and imaginary part. Indeed, in analyzing the shift of the plasma resonance in the optical properties for small metal particles[145], L.Genzel and T.P Martin used the changes of frequency-dependent complex dielectric functions in the local neighborhood of small metal particle exhibiting a uniform mode plasmon resonance an given by the classical dipole approximation through the one single Lorentzian oscillator dipole functions[1, 151, 6], which analytically is given in equation (9) as a photon energy function.

$$\varepsilon_r(E) = 1 - \sum_j \frac{A_j}{{E_0}^2{}_j - E^2 + i\Gamma_j E} \quad (9)$$

Where A_j, E_o, E and, Γ denote oscillator strength, resonance photon energy, photon energy and damping coefficient, respectively. The complex dielectric is described as sum of different oscillators and the subscript j depicts the jth oscillator. The energy-dependent imaginary part form of equation (3) is often referred to as Lorentzian. Fundamentally, the Lorentz model assumes a physical model in which the electron oscillates in viscous fluid[15] and account the inter-band transition

contributions. The phase and amplitude of electric dipole are obtained by equation (10) and (c), respectively:

$$\delta_{dip} = \tan^{-1}\left(-\frac{\Gamma E}{{E_0}^2 - E^2}\right) \quad (10)$$

The amplitude of electric dipole:

$$a_{dip} = \frac{1}{\left[\left({E_0}^2 - E^2\right)^2 - \Gamma^2 E^2\right]^{\frac{1}{2}}} \quad (11)$$

Approximately for the scattering first and second derivatives, the oscillator phases of electric dipole were obtained by equation (d):

$$\delta_{dip} = \tan^{-1}\left[-\frac{\mathrm{Im}[\varepsilon(\omega)]}{\mathrm{Re}[\varepsilon(\omega)]}\right] \approx \tan^{-1}\left[\frac{\frac{dI_{scat.}}{d\omega}}{I_{scat}}\right] \quad (12)$$

The LSPR quality factor is obtained by the equation (13)

$$Q_{LSPR} = \frac{\left|\mathrm{Re}[\varepsilon(E)]\right|}{\mathrm{Im}[\varepsilon(E)]} \quad (13)$$

The second member of equation (12) is the phase-like in terms or derivations for Lorentzian-like signal.

Noise Analysis

Unfortunately, noise-free data can never be realized in laboratory because some types of noise arise from thermodynamic and quantum effects that are impossible to avoid in a measurement[16]. In traditional LSPR based sensing experiment, monitoring shifts of the peak position in response to local refractive index (RI) changes is limited by instrumental and chemical noise, due to the limited ability of resolving minute shifts changes in the LSPR position peak and shape, so-called broadening and asymmetry. Noise associated with our experiment data, especially the LSPR scattering peak maxima depicted by capital B (Figure 2A,the first line),

inflexion points A and C in the local air, water and oil RI media. As it can be seen from the tables S1 and S2 the method did not propagate the noise significantly.

References

1. Olson, J.; Dominguez-Medina, S.; Hoggard, A.; Wang, L.-Y.; Chang, W.-S.; Link, S., Optical characterization of single plasmonic nanoparticles. Chemical Society Reviews 2015,44 (1), 40-57.
2. Amendola, V.; Pilot, R.; Frasconi, M.; Marago, O. M.; Iati, M. A., Surface plasmon resonance in gold nanoparticles: a review. Journal of physics. Condensed matter : an Institute of Physics journal 2017,29 (20), 203002.
3. Lombardi, A.; Loumaigne, M.; Crut, A.; Maioli, P.; Del Fatti, N.; Vallee, F.; Spuch-Calvar, M.; Burgin, J.; Majimel, J.; Treguer-Delapierre, M., Surface plasmon resonance properties of single elongated nano-objects: gold nanobipyramids and nanorods. Langmuir : the ACS journal of surfaces and colloids 2012,28 (24), 9027-33.
4. Baida, H.; Billaud, P.; Marhaba, S.; Christofilos, D.; Cottancin, E.; Crut, A.; Lerme, J.; Maioli, P.; Pellarin, M.; Broyer, M.; Del Fatti, N.; Vallee, F.; Sanchez-Iglesias, A.; Pastoriza-Santos, I.; Liz-Marzan, L. M., Quantitative determination of the size dependence of surface plasmon resonance damping in single Ag@SiO(2) nanoparticles. Nano letters 2009,9 (10), 3463-9.
5. Polavarapu, P. L., Kramers-Kronig transformation for optical rotatory dispersion studies. The journal of physical chemistry. A 2005,109 (32), 7013-23.
6. Keefe, C. D., Curvefitting Imaginary Components of Optical Properties: Restrictions on the Lineshape Due to Causality. Journal of Molecular Spectroscopy 2001,205 (2), 261-268.
7. Dressel, M.; Gompf, B.; Faltermeier, D.; Tripathi, A. K.; Pflaum, J.; Schubert, M., Kramers-Kronig-consistent optical functions of anisotropic crystals: generalized spectroscopic ellipsometry on pentacene. Opt. Express 2008,16 (24), 19770-19778.
8. Haes, A. J.; Zou, S.; Zhao, J.; Schatz, G. C.; Van Duyne, R. P., Localized surface plasmon resonance spectroscopy near molecular resonances. J Am Chem Soc 2006,128 (33), 10905-14.

9. Polavarapu, P. L.; Petrovic, A. G.; Zhang, P., Kramers-Kronig transformation of experimental electronic circular dichroism: application to the analysis of optical rotatory dispersion in dimethyl-L-tartrate. Chirality 2006,18 (9), 723-32.
10. Hall, S. H.; Heck, H. L., Advanced Signal Integrity for High-Speed Digital Designs. Wiley-IEEE Press: 2009; p 660.
11. Akyurtlu, A.; Kussow, A.-G., Relationship between the Kramers-Kronig relations and negative index of refraction. 2010; Vol. 82.
12. Gorkunov, M. V.; Dmitrienko, V. E.; Ezhov, A. A.; Artemov, V. V.; Rogov, O. Y., Implications of the causality principle for ultra chiral metamaterials. Scientific Reports 2015,5, 9273.
13. Lovell, R., Application of Kramers-Kronig relations to the interpref(-ço—kkç çnnkçknçtation of dielectric data. Journal of Physics C: Solid State Physics 1974,7 (23), 4378.
14. Genzel, L.; Martin, T. P.; Kreibig, U., Dielectric function and plasma resonances of small metal particles. Zeitschrift für Physik B Condensed Matter 1975,21 (4), 339-346.
15. Bohren, C. F.; Huffman, D. R., Absorption and Scattering by an Arbitrary Particle. In Absorption and Scattering of Light by Small Particles, Wiley-VCH Verlag GmbH: 2007; pp 57-81.
16. Skoog, D. A.; Crouch, S. R.; Holler, F. J., Principles of instrumental analysis. Thomson Brooks/Cole: Belmont, CA, 2007.

Supporting Tables: Inflection points and LSPR locations on the curvatures in various refractive indexes and sensitivities.

Single AuBPs	1	2	3	4	5	6	7	8	9	10	Ave.	Std.
Inflection A (eV)	1.72	1.80	1.69	1.79	1.85	1.74	1.80	1.83	1.74	1.82	1.78	0.05
LSPR B (eV)	1.76	1.84	1.74	1.84	1.90	1.78	1.84	1.87	1.78	1.86	1.82	0.05
Inflection C (eV)	1.79	1.88	1.78	1.89	1.95	1.82	1.88	1.91	1.82	1.90	1.86	0.06

Table S1. *Air*

Single AuBPs	1	2	3	4	5	6	7	8	9	10	Ave.	Std.
Inflection A (eV)	1.68	1.63	1.61	1.66	1.72	1.67	1.66	1.65	1.64	1.64	1.66	0.03
LSPR B (eV)	1.72	1.66	1.67	1.69	1.77	1.70	1.69	1.68	1.68	1.67	1.69	0.03
Inflection C (eV)	1.75	1.70	1.73	1.72	1.81	1.74	1.73	1.72	1.71	1.71	1.73	0.03

Table S2. *Water*

Single AuBPs	1	2	3	4	5	6	7	8	9	10	Ave.	Std.
Inflection A (eV)	1.54	1.57	1.47	1.57	1.54	1.54	1.56	1.55	1.55	1.58	1.55	0.03
LSPR B (eV)	1.56	1.60	1.50	1.60	1.57	1.57	1.59	1.58	1.58	1.61	1.58	0.03
Inflection C (eV)	1.59	1.63	1.53	1.63	1.60	1.60	1.62	1.62	1.60	1.64	1.61	0.03

Table S3. *Oil*

Single AuBPs	1	2	3	4	5	6	7	8	9	10	Ave.	Std.
Slope at Inflection A ($eV \cdot RIU^{-1}$)	0.32	0.45	0.41	0.42	0.58	0.37	0.46	0.54	0.36	0.48	0.44	0.080
Slope at LSPR B ($eV \cdot RIU^{-1}$)	0.36	0.48	0.44	0.47	0.61	0.39	0.48	0.56	0.38	0.50	0.47	0.080
Slope at Inflection C ($eV \cdot RIU^{-1}$)	0.36	0.49	0.45	0.51	0.65	0.41	0.50	0.56	0.42	0.51	0.49	0.080

Table S4. *Sensitivities*

Supporting Figures

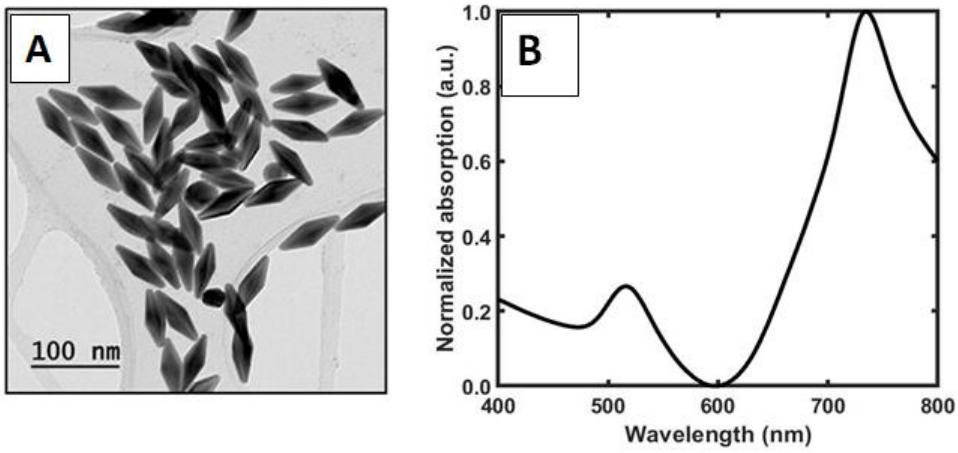

Figure S1. *Characterization of gold bipyramids (AuBPs) used in this study.(A) Scanning electron microscope (SEM) image of AuBPs (B) High energy transverse*

peak and low energy longitudinal peak of the absorption spectrum of an ensemble AuBPs sample.

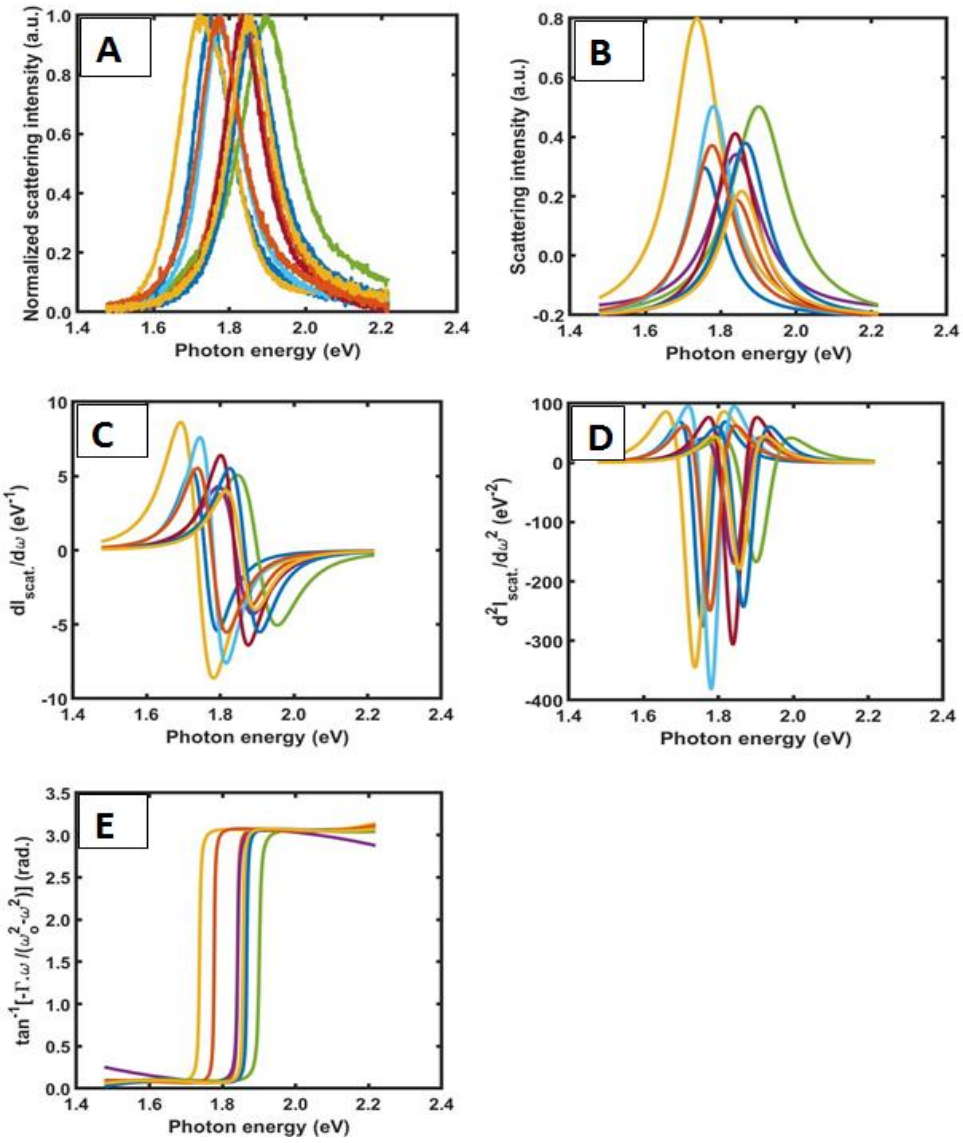

Figure S2. *Plotted data of LSPR of single AuBPs (A) and their fitted curves (B), First (C) and Second (D) derivatives and Scattering phases (E) for air refractive index medium.*

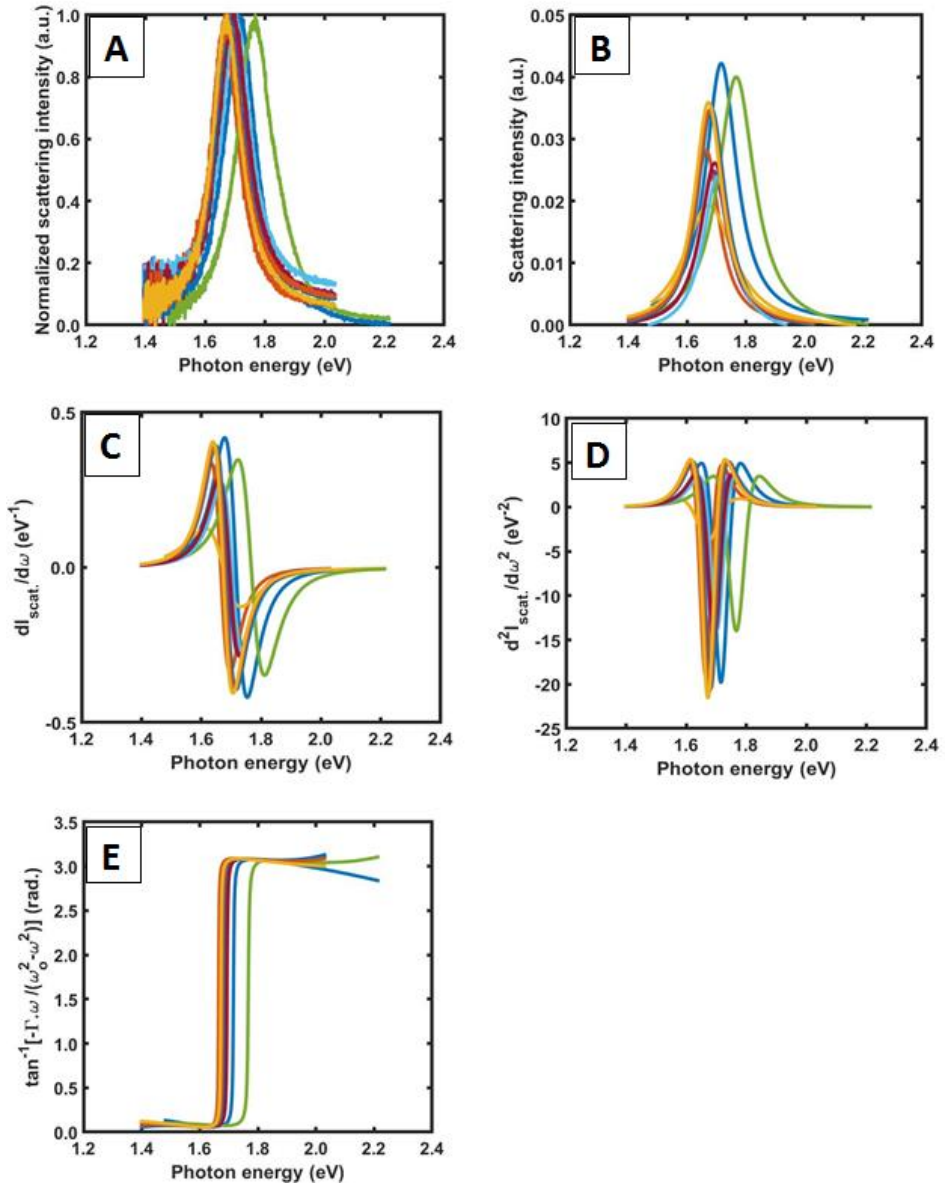

Figure S3. *Plotted data of LSPR of single AuBPs (A) and their fitted curves (B), First (C) and Second (D) derivatives and Scattering phases (E) for water refractive indexes.*

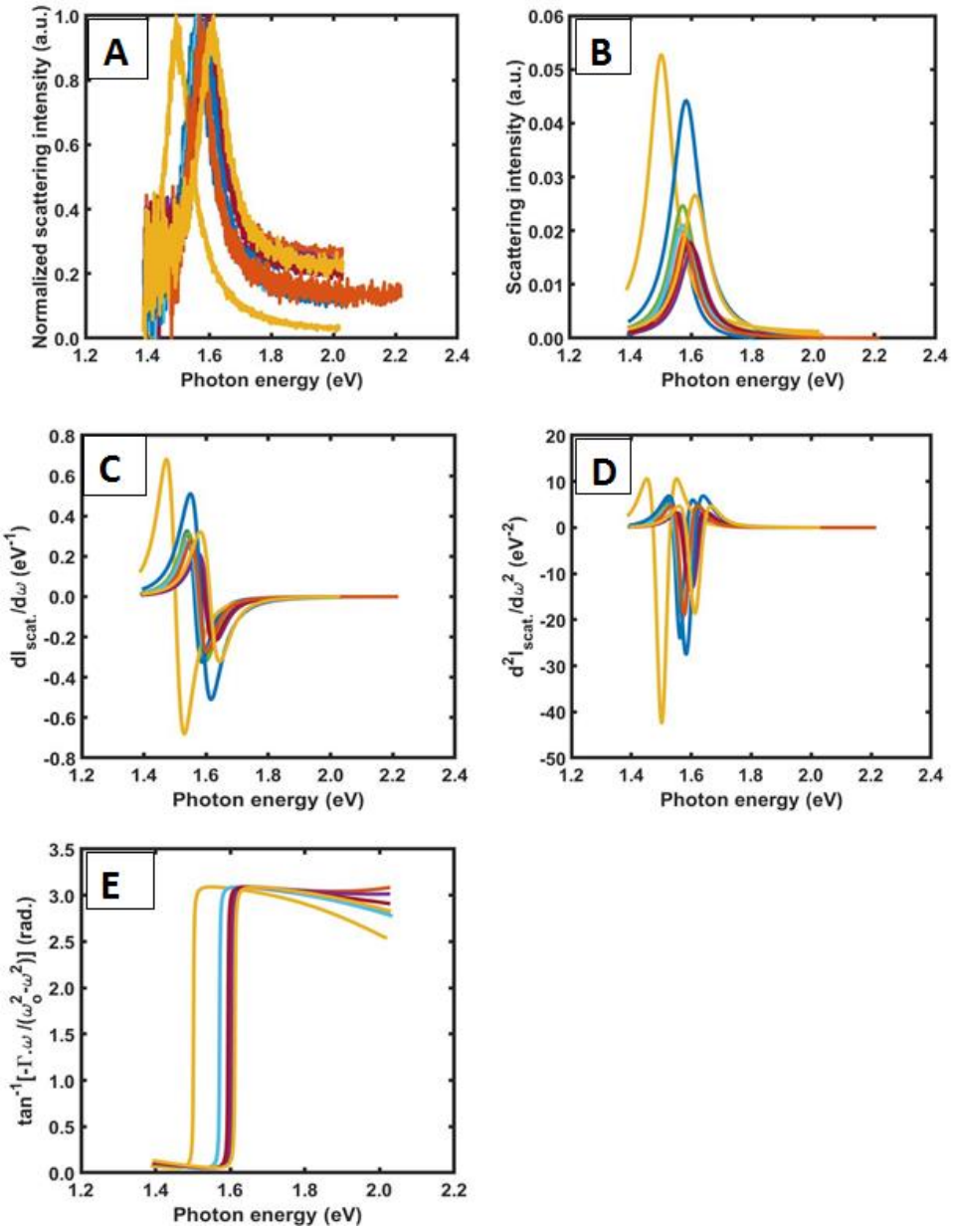

Figure S4. *Plotted data of LSPR of single AuBPs (A) and their fitted curves (B), First (C) and Second (D) derivatives and Scattering phases (E) for oil refractive indexes.*

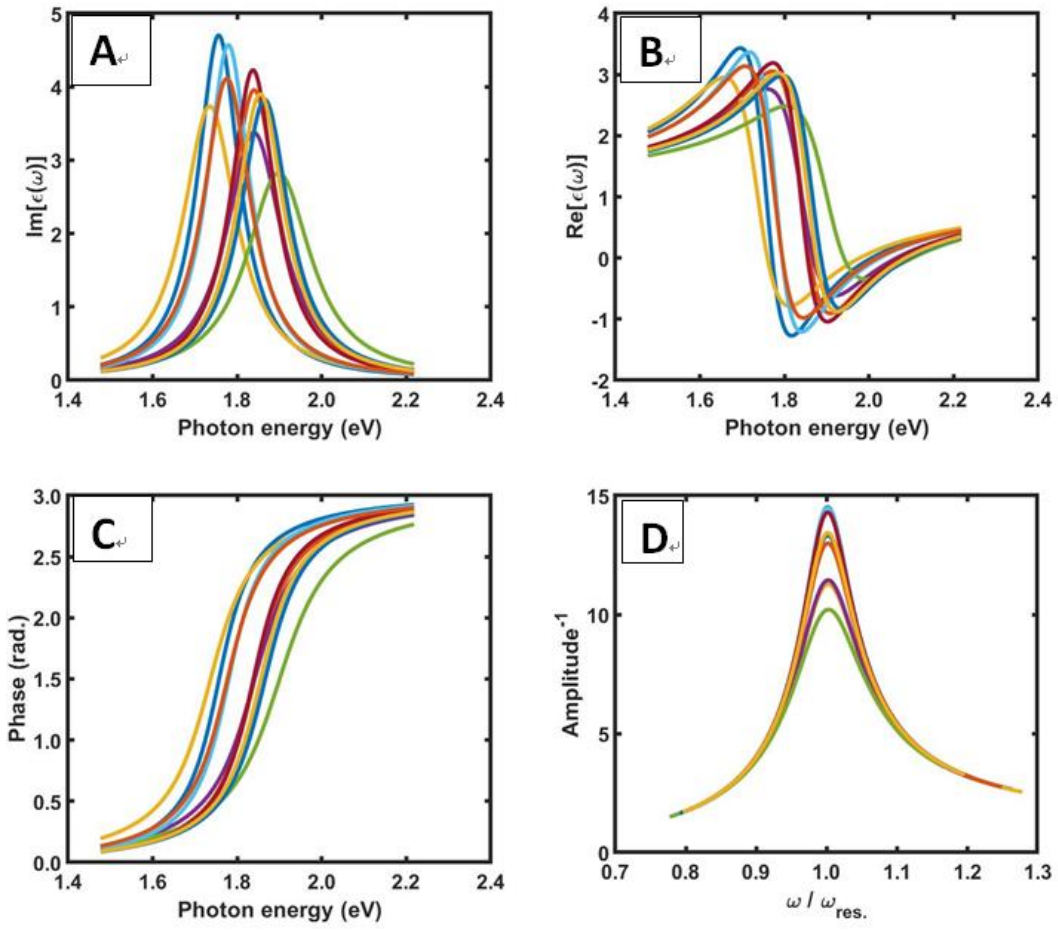

Figure S5. *Plotted data of Im[ε(ω)] (A), Re[ε(ω)] (B), Phase of dipole (C) and Amplitude (D) for changes of complex dielectric functions for air refractive index.*

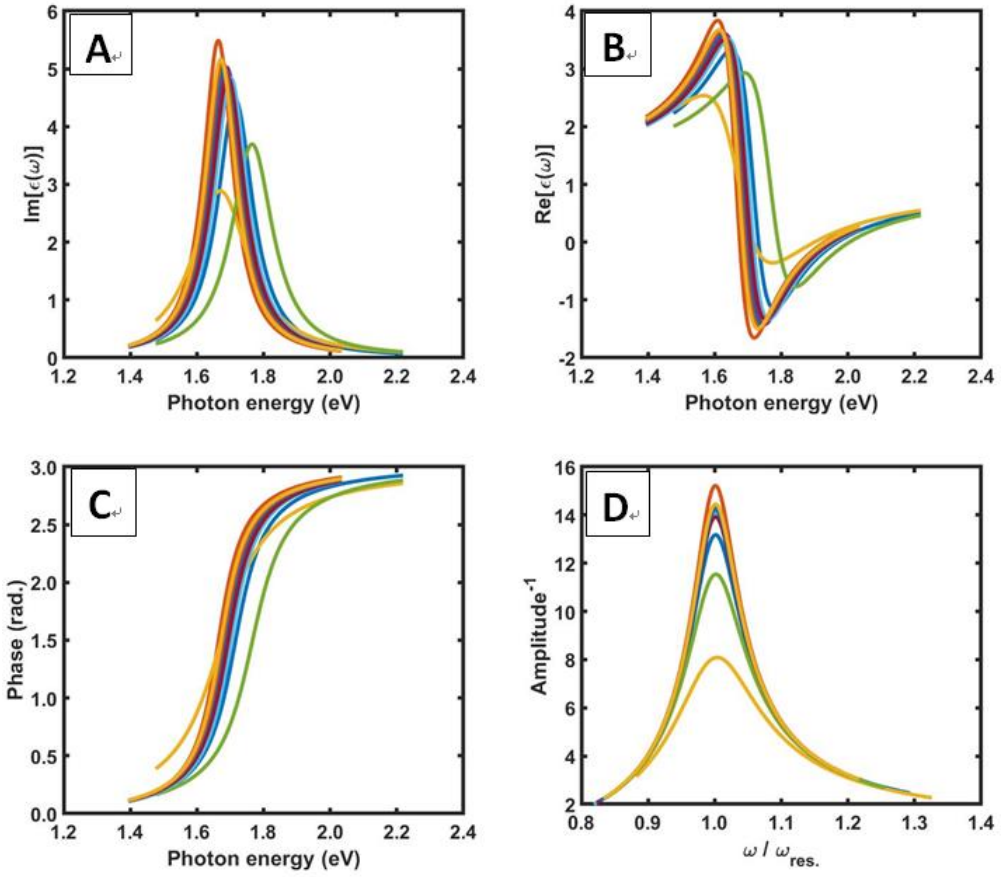

Figure S6. *Plotted data of Im[ε(ω)] (A), Re[ε(ω)] (B), Phase of dipole (C) and Amplitude (D) for changes of complex dielectric functions for water refractive index.*

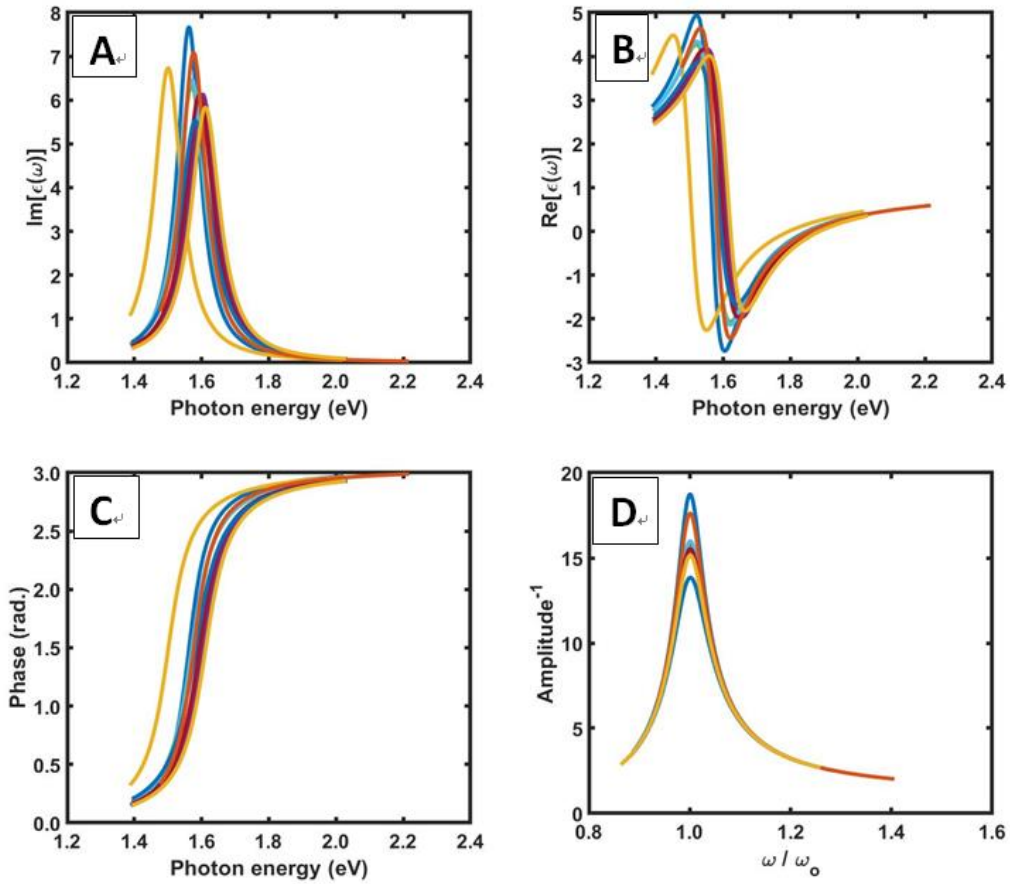

Figure S7. *Plotted data of Im[ε(ω)] (A), Re[ε(ω)] (B), Phase of dipole (C) and Amplitude (D) for changes of complex dielectric functions for oil refractive index.*

CHAPTER 4: GENERAL CONCLUSION AND FUTURE WORKS

In conclusion, anisotropic single AuNPs and corresponding curvatures of their LSPRs are utilized to investigate on the enhancement of the LSPRs sensitivities. Two LSPR IFs, high and low sensitive with respect to the LSPR peak maximum sensitivities are found. The LSPRs IF also showed useful characteristics for probing the dispersive nature of tunable complex RI in the visible range. The LSPR IFs probing the dispersive nature of tunable complex RI is undergoing further investigations.